

# **The *Legionella*-driven PtdIns(4)*P* gradient at LCV-ER membrane contact sites promotes Vap-, OSBP- and Sac1-dependent pathogen vacuole remodeling**

**Simone Vormittag<sup>1</sup>, Dario Hüsler<sup>1</sup>, Ina Haneburger<sup>1</sup>, Tobias Kroniger<sup>2</sup>, Aby Anand<sup>3</sup>, Manuel Prantl<sup>1</sup>, Caroline Barisch<sup>3</sup>, Sandra Maaß<sup>2</sup>, Dörte Becher<sup>2</sup>, François Letourneur<sup>4</sup> & Hubert Hilbi<sup>1\*</sup>**

<sup>1</sup>Institute of Medical Microbiology, University of Zürich, Gloriastrasse 30, 8006 Zürich, Switzerland.

<sup>2</sup>Institute of Microbiology, University of Greifswald, Felix-Hausdorff-Strasse 8, 17489 Greifswald, Germany.

<sup>3</sup>Division of Molecular Infection Biology and Center for Cellular Nanoanalytics, University of Osnabrueck, Barbarastrasse 13, 49076 Osnabrueck, Germany.

<sup>4</sup>Laboratory of Pathogen Host Interactions, Université de Montpellier, CNRS, INSERM, Place Eugène Bataillon, Montpellier, 34095, cedex 5, France.

**Running title:** LCV remodeling through ER membrane contact sites

**Key words:** Amoeba, atlastin, *Dictyostelium discoideum*, large fusion GTPase, host-pathogen interaction, *Legionella pneumophila*, Legionnaires' disease, oxysterol binding protein, pathogen vacuole.

**Abbreviations:** ATL, Atlastin, FFAT motif, two phenylalanines (FF) in an acidic tract motif; Icm/Dot, intracellular multiplication/defective organelle trafficking; IFC, imaging flow cytometry; LCV, *Legionella*-containing vacuole; GFP, green fluorescent protein; MCS, membrane contact sites; OSBP, oxysterol binding protein; T4SS, type IV secretion system; VAMP, vesicle-associated membrane protein; Vap, VAMP-associated protein.

**\*Correspondence:** hilbi@imm.uzh.ch; Tel.: +41 (0)44 634 2650

## 27 Abstract

28 The causative agent of Legionnaires' disease, *Legionella pneumophila*, governs interactions  
 29 with host cells by secreting ca. 330 different "effector" proteins. The facultative intracellular  
 30 bacteria replicate in macrophages and amoeba within a unique compartment, the *Legionella*-  
 31 containing vacuole (LCV). Hallmarks of LCV formation are the phosphoinositide (PI) lipid  
 32 conversion from PtdIns(3)*P* to PtdIns(4)*P*, fusion with endoplasmic reticulum (ER)-derived  
 33 vesicles and a tight association with the ER. Proteomics of purified LCVs revealed the  
 34 presence of membrane contact sites (MCS) proteins implicated in lipid exchange. Using  
 35 dually fluorescence-labeled *Dictyostelium discoideum* amoeba, we reveal that the VAMP-  
 36 associated protein (Vap), the PtdIns(4)*P* 4-phosphatase Sac1, and the large fusion GTPase  
 37 Sey1/atlastin-3 localize to the ER, but not to the LCV membrane, and that these ER-resident  
 38 proteins promote intracellular replication of *L. pneumophila* and LCV remodeling. Moreover,  
 39 oxysterol binding proteins (OSBPs) preferentially localize to the ER (OSBP8) or the LCV  
 40 membrane (OSBP11), respectively, and promote (OSBP8) or restrict (OSBP11) intracellular  
 41 replication of *L. pneumophila* and LCV expansion. Furthermore, the PtdIns(4)*P*-subverting *L.*  
 42 *pneumophila* effectors LepB and SidC also promote LCV remodeling. Taken together, the  
 43 *Legionella*- and host cell-driven PtdIns(4)*P* gradient at LCV-ER MCSs promotes Vap-,  
 44 OSBP- and Sac1-dependent pathogen vacuole remodeling.

45

## 46 Introduction

47 *Legionella pneumophila* is an amoeba-resistant environmental bacterium, which causes a  
 48 severe pneumonia called Legionnaires' disease [1, 2]. The facultative intracellular pathogen  
 49 employs a conserved mechanism to grow in free-living protozoa as well as in alveolar  
 50 macrophages, which is a prerequisite to cause disease [3-6]. To govern the interaction with  
 51 host cells, *L. pneumophila* employs the Icm/Dot (Intracellular multiplication/defective  
 52 organelle trafficking) type IV secretion system (T4SS), which translocates ca. 330 different

53 “effector” proteins into host cells [6, 7]. These effector proteins subvert pivotal host cell  
54 processes, including the endocytic, secretory, retrograde and autophagy pathways, lipid  
55 metabolism, transcription, translation, and apoptosis [8-12].

56 Within host cells, *L. pneumophila* forms a unique, membrane-bound replication  
57 compartment, the *Legionella*-containing vacuole (LCV), which restricts interactions with the  
58 endocytic pathway [13-16]. Hallmarks of LCV formation are the phosphoinositide (PI) lipid  
59 conversion from phosphatidylinositol 3-phosphate (PtdIns(3)*P*) to PtdIns(4)*P*, the subversion  
60 of the small GTPase Rab1, fusion of the pathogen vacuole with endoplasmic reticulum (ER)-  
61 derived vesicles, and finally, a tight association with the ER [13-16]. The LCV is decorated  
62 with PtdIns(4)*P* [17], and PI conversion from the endocytic PI PtdIns(3)*P* to the secretory PI  
63 PtdIns(4)*P* occurs in the first 1-2 hours after bacterial uptake [18].

64 The production of PtdIns(4)*P* on the LCV membrane implicates the sequential activity of  
65 *L. pneumophila* Icm/Dot-secreted effector proteins: PtdIns 3-kinase MavQ [19], PtdIns(3)*P* 4-  
66 kinase LepB [20] and PtdIns(3,4)*P*<sub>2</sub> 3-phosphatase SidF [21]. Moreover, host PI-modulating  
67 enzymes such as the PtdIns 4-kinases PI4KIIIα [22] and PI4KIIIβ [23], and the PtdIns(4,5)*P*  
68 5-phosphatase OCRL1 [24] might also play a role in the production of PtdIns(4)*P* on the LCV  
69 membrane.

70 The small GTPase Rab1 is enriched in the *cis*-Golgi apparatus and controls ER-Golgi  
71 secretory trafficking [14]. Rab1 is recruited to the LCV membrane and activated by the  
72 Icm/Dot secreted effector SidM (*alias* DrrA), which binds to PtdIns(4)*P* through the novel  
73 P4M domain [22, 23, 25-27] and possess Rab1 guanine nucleotide exchange factor (GEF)/  
74 guanine dissociation inhibitor (GDI) displacement factor (GDF) activity [28-34] as well as  
75 adenosine monophosphorylation (AMPylation) activity [35, 36]. Moreover, Rab1 is de-  
76 AMPylated by the effector SidD [37, 38] and reversibly phosphocholinated by the effectors  
77 AnkX and Lem3 [39-41]. The covalent modifications of GTP-bound Rab1 lock the small  
78 GTPase in its active state. Finally, Rab1 is inactivated by the GTPase activating protein

(GAP) LepB [31]. The small GTPase ARF1 controls also retrograde Golgi-ER trafficking [14]. ARF1 is recruited to and activated on the LCV by the effector RalF, the first *L. pneumophila* GEF identified [42].

The LCV intercepts trafficking at ER exit sites between the ER and the Golgi apparatus, and inhibition of ER-Golgi transport blocks the formation of the pathogen vacuole [42-44]. Sec22b, a SNARE (soluble *N*-ethylmaleimide-sensitive factor (NSF) attachment protein (SNAP) receptor), which promotes fusion of ER-derived vesicles with the *cis*-Golgi, is recruited to LCVs shortly after infection [45, 46]. The activation of Rab1 by SidM on the LCV mediates the fusion of ER-derived vesicles with the pathogen vacuole through the non-canonical pairing of the vesicle (v-)SNARE Sec22b on the vesicles with plasma membrane (PM)-derived target (t-)SNAREs such as syntaxin (Stx) 2, 3, 4 and SNAP23 on the LCV [47, 48]. The LCV intercepts anterograde as well as retrograde trafficking between the ER and the Golgi apparatus [9, 11, 13, 14]. Accordingly, nascent LCVs continuously capture and accumulate PtdIns(4)*P*-positive vesicles from the Golgi apparatus, and their sustained association requires a functional T4SS [49]. LCVs also sequentially recruit the small GTPases Rab33b, Rab6a and the ER-resident SNARE syntaxin18 (Stx18), which are implicated in Golgi-ER retrograde trafficking, to promote the association of the pathogen vacuole with the ER [50].

The association of the LCV with ER in macrophages and amoeba has been initially documented more than 25 years ago [51, 52]. The vacuole containing *L. pneumophila* associates with rough ER within minutes after uptake, and dependent on the Icm/Dot T4SS, the vacuole and the ER form extended contact sites (> 0.5  $\mu$ m in length), which are connected by tiny, periodic “hair-like” structures [53]. Remarkably, the ER elements remain attached to LCVs even after cell homogenization [53], and intact LCVs purified from *L. pneumophila*-infected *D. discoideum* co-purify with extensive fragments of calnexin-GFP-positive ER [54-56]. In dually fluorescence labeled *D. discoideum*, LCVs accumulate calnexin-positive ER

within minutes, and the ER remains separate from the PtdIns(4)*P*-positive pathogen vacuole for at least 8 h post infection [18, 57]. The ER tubules interacting with LCVs are decorated with reticulon 4 (Rtn4) and the large fusion GTPase atlastin/Sey1, which are implicated in the architecture and dynamics of the ER, respectively [58, 59]. The *L. pneumophila* effector Ceg9 might stabilize the LCV-ER contact sites by directly binding to the host protein Rtn4 [58]. Finally, depletion of the PtdIns(4)*P* 4-phosphatase Sac1, a crucial enzyme of ER membrane contact sites (MCS), reduced the recruitment of endogenous Rab1 to LCVs [22].

The MCS between two distinct cellular compartments or organelles adopt a number of functions and are of crucial importance for the non-vesicular exchange of lipids in mammalian cells [60]. MCS between the ER and the PM or organelles promote lipid exchange driven by a gradient of PtdIns(4)*P*, which is established by PtdIns 4-kinases on the PM or organelles and maintained by the integral ER membrane protein PtdIns(4)*P* 4-phosphatase Sac1 [61, 62]. Driven by the PtdIns(4)*P* gradient, phosphatidylserine accumulates at the inner leaflet of the PM [63, 64] and cholesterol accumulates at the Golgi apparatus [61, 65]. The lipid exchange is promoted by lipid transfer proteins termed oxysterol binding proteins (OSBPs), several of which bind PtdIns(4)*P* through a PH domain and by the ER-resident Vap (vesicle-associated membrane protein (VAMP)-associated protein) through a FFAT (two phenylalanines (FF) in an acidic tract) motif [60].

Given the accumulation of PtdIns(4)*P* on the limiting LCV membrane and the tight association of the pathogen vacuole with ER, the LCV-ER interface might actually form a functionally important MCS, which promote pathogen vacuole remodeling through a PtdIns(4)*P* gradient. Using dually fluorescence-labeled *D. discoideum* amoeba, we identify Vap, Sac1 and Sey1 on the ER, but not on the LCV membrane, while OSBP8 and OSBP11 exclusively localize to the ER or the LCV membrane, respectively. The MCS components are implicated in LCV remodeling and intracellular growth of *L. pneumophila*, and a LCV-to-ER PtdIns(4)*P* gradient is established by bacterial effector proteins. These findings indicate that

the *Legionella*-driven PtdIns(4)*P* gradient at LCV-ER MCSs promotes Vap-, Sac1- and OSBP-dependent pathogen vacuole remodeling.

## Results

### Comparative proteomics of LCVs from *D. discoideum* wild-type and $\Delta$ *sey1* reveals MCS components

Given the tight and stable association of the LCV limiting membrane with the ER, MCS are likely formed between the compartments. The ER tubule-resident large GTPase Sey1/Atl3 (DDB\_G0279823) promotes the decoration of LCVs with ER, and in absence of the GTPase, significantly less ER accumulates on the pathogen vacuole, while the PtdIns(4)*P*-positive LCV appears to form normally [59, 66]. To gain further insights into the process of LCV formation, and in particular the role of the ER, we analyzed by comparative proteomics LCVs from the *L. pneumophila*-infected *D. discoideum* Ax3 wild-type strain or the  $\Delta$ *sey1* mutant. This approach revealed 3658 host or bacterial proteins identified on LCVs from *D. discoideum* Ax3 or  $\Delta$ *sey1* (**Table S1**).

These proteins include the OSBPs OSBP7 (*osbG*) and OSBP8 (*osbH*), the PtdIns(4)*P* 4-phosphatase Sac1, the hydrolase receptor sortilin, the ER proteins calnexin, calmodulin, calreticulin and reticulon, the ER-Golgi intermediate compartment protein-3 (Ergic3), the Golgi proteins golgesin and YIPF1, the vesicle transport through interaction with t-SNAREs homolog 1A (Vti1A), the vesicle-associated membrane protein-7A/B (Vamp7A/B), the vesicle-fusing ATPase (NsfA), the vacuolar protein sorting-associated proteins Vps26, Vps29, and Vps35 (retromer coat complex subunits), dynamin A/B (DymA/B), dynamin-like protein A/C (DlpA/C), Vps4, Vps11, Vps13A, Vps16, Vps45, Vps51, Vps53, syntaxins (5, 7A/B, 8A/B), t-SNAREs, synaptobrevin B,  $\alpha$ -SNAP, and many small GTPases or their modulators (Arf1, Arf1 GEF, Arl8, Rab1A/B/C/D, Rab2A/B, Rab4, Rab5A/B, Rab6, Rab7A, Rab8A, Rab11A/C, Rab14, Rab18, Rab21, Rab32A/B/C/D, RabC, RabJ, RabG2, RabQ, Rab GDI,

Rac1A, RacB, RacE, RagA, RanA, RanBP1, RasB, RasC, RasG, RasS, RapA, Rap GAP, Rho GAP, Rho GDI, Sar1, Spg1), as well as the interaptin AbpD [67], the metal ion transporter Nramp1 [68, 69], and the GPCR and receptor protein kinase RpkA [70]. Moreover, many mitochondrial proteins were found to associate with LCVs (**Table S1**). Finally, the *L. pneumophila* PtdIns 4-kinase LepB [20], the PtdIns(4)*P*-binding effectors SidC, its paralogue SdcA, and SidM/DrrA [17, 23, 71], as well as the retromer interactor RidL [72] and the deAMPyase SidD [37, 38] were also identified on LCVs from *D. discoideum* Ax3 and  $\Delta$ *sey1* (**Table S1**).

Furthermore, 74 *D. discoideum* or 34 *L. pneumophila* proteins were identified only on LCVs from *D. discoideum* Ax3, while 11 host and 3 bacterial proteins were present only on LCVs from  $\Delta$ *sey1* mutant amoeba (**Fig. 1A, Table S1**). Among the host proteins present only on LCVs from *D. discoideum* Ax3, we identified several putative MCS components possibly involved in (PI-driven) lipid transport (OSBP7, Vps13B, CRAL-TRIO domain protein), as well as proteins possibly implicated in ER-Golgi transport (TRAPPC3, YIPF5,  $\gamma$ -SNAP), or localizing to the ER (syntaxin18, calmodulin, Sey1) (**Table S1**). Among the *L. pneumophila* proteins identified only on LCVs from *D. discoideum*  $\Delta$ *sey1* was the PtdIns(4)*P*-binding effector Lpg2603 [73] (**Table S1**). Based on these findings, we sought to analyze *D. discoideum* factors possibly involved in LCV-ER MCS.

*D. discoideum* harbors single putative orthologues of the PtdIns(4)*P* 4-phosphatase Sac1 (DDB\_G0271630), and the VAMP-associated protein (Vap; DDB\_G0278773), as well as several OSBPs, including OSBP7 (DDB\_G0283035; *osbG*), OSBP8 (DDB\_G0283709; *osbH*) and OSBP11 (DDB\_G0288817; *osbK*). All 12 *D. discoideum* OSBPs belong to the class of “short OSBPs”, which harbor a putative lipid-binding ORD domain (OSBP-related domain) but lack ankyrin repeats (protein-protein interaction), a PH domain (PI binding), a trans-membrane domain (TMD; membrane interaction), and the FFAT motif (Vap interaction) (**Fig. S1**). OSBP8 and OSBP11 are most similar to one another and most closely related to human



short OSBPs. OSBP7 represents an OSBP more distantly related to the other paralogues, and OSBP1 (*osbA*), OSBP2 (*osbB*), OSBP3 (*osbC*), OSBP5 (*osbE*) and OSBP6 (*osbF*) form a separate cluster.

In order to validate the localization of MCS components to LCVs, GFP fusion proteins of Vap, OSBP7, OSBP8, OSBP11 or Sac1 were co-produced alongside the PtdIns(4)*P*/LCV probe P4C-mCherry [59] in *D. discoideum* Ax3 or  $\Delta$ *sey1*, and their localization to LCVs was assessed by imaging flow cytometry (IFC) (**Fig. 1B**). All putative MCS components were found to localize to PtdIns(4)*P*-positive LCVs, and Vap accumulated on significantly fewer LCVs in  $\Delta$ *sey1* mutant amoeba. Since IFC has a rather low spatial resolution, the PtdIns(4)*P*-positive limiting LCV membrane cannot be discriminated from tightly associated ER. In summary, comparative proteomics identified MCS components on purified LCVs, the localization of which to the pathogen vacuole was confirmed by IFC.

# ***D. discoideum* MCS components localize to the ER or the LCV membrane**

Based on the above bioinformatic and experimental considerations, we sought to analyze the role of the putative MCS components Vap, OSBP7, OSBP8, OSBP11 and Sac1 for LCV formation and the LCV-ER MCS in detail. Using dually fluorescently labeled *D. discoideum*, we assessed by confocal fluorescence microscopy the co-localization of GFP fusions of Vap, OSBP7, OSBP8, OSBP11 or Sac1 with either the ER-resident protein calnexin A-mCherry (CnxA-mCherry), the PtdIns(4)*P*/LCV probe P4C-mCherry, or the endosomal transporter AmtA-mCherry (**Fig. 2A, Fig. S2A**). This high-resolution approach revealed that Vap and OSBP8, but significantly less OSBP7 and OSBP11, co-localize with CnxA-mCherry in *L. pneumophila*-infected (**Fig. 2B**) as well as in uninfected amoeba (**Fig. S2B-D**). The PtdIns(4)*P* 4-phosphatase Sac1 and its catalytically inactive mutant, Sac1\_C383S, also co-localized with CnxA-mCherry, while a Sac1 variant lacking the ER-targeting transmembrane domain, Sac1\_ΔTMD, diffusely localized throughout the cell (**Fig. 2B**). Moreover, Vap and



OSBP11 co-localized with P4C-mCherry, while OSBP7, OSBP8 and Sac1 did not (**Fig. 2C**), and Vap and OSBP11 also co-localized with AmtA-mCherry more extensively than the other MCS components (**Fig. 2D**). Finally, OSBP11 intensely localized to the PM. In summary, Vap, OSBP8 and Sac1 co-localize with ER-resident CnxA-mCherry, and Vap as well as OSBP11 co-localize with the PtdIns(4)*P* probe P4C-mCherry and the endosomal/LCV marker AmtA-mCherry (**Table 1**). Hence, at LCV-ER MCS Vap localizes to LCVs as well as to the ER, while OSBP8 and Sac1 preferentially localize to the ER, and OSBP11 preferentially localizes to LCVs.

# **MCS components modulate the replication of *L. pneumophila* in *D. discoideum* and mammalian cells**

To further assess the role of the MCS components for intracellular replication of *L. pneumophila* and LCV formation, we constructed *D. discoideum* deletion mutant strains lacking *vap*, *osbG*, *osbH* or *osbK* by disrupting the corresponding genes with a blasticidin selection marker (**Fig. S3**). Several independent clones of the deletion mutants were picked and further analyzed. Despite repeated attempts, we failed to obtain a  $\Delta$ *sacI* deletion mutant, and therefore, the gene might be essential in *D. discoideum*. Instead, we constructed and used a dominant negative Sac1 variant lacking the ER-targeting transmembrane domain, Sac1\_ $\Delta$ TMD, and the catalytically inactive Sac1\_C383S mutant.

To assess the role of these putative MCS components for intracellular replication of *L. pneumophila*, we used mCherry-producing bacteria and quantified fluorescence intensity (RFU) (**Fig. 3**) and colony forming units (CFU) (**Fig. S4A**). We compared intracellular growth of the wild-type *L. pneumophila* strain JR32 in *D. discoideum*  $\Delta$ *vap*, as well as in the  $\Delta$ *osbG*,  $\Delta$ *osbH*, and  $\Delta$ *osbK* mutant strains (**Fig. 3A**). In *D. discoideum*  $\Delta$ *vap*, intracellular bacterial growth was reduced at 4-8 days post infection (p.i.) and enhanced at 10 days p.i. Moreover, intracellular bacterial growth was enhanced in *D. discoideum*  $\Delta$ *osbH*, reduced in

$\Delta osbK$  and not affected in  $\Delta osbG$ . The intracellular growth phenotypes of *L. pneumophila* in the *D. discoideum*  $\Delta vap$ ,  $\Delta osbH$  and  $\Delta osbK$  mutants were reverted by expressing the corresponding genes on a plasmid (**Fig. 3A**). The intracellular growth of *L. pneumophila* strain JR32 was similar in *D. discoideum* Ax3 producing GFP, GFP-Sac1 or GFP-Sac1\_C383S but significantly reduced in amoeba producing GFP-Sac1\_ΔTMD (**Fig. 3B, Fig. S4A**). These results are in agreement with the notion that Sac1 is implicated in intracellular growth of *L. pneumophila*, and Sac1\_ΔTMD but not GFP-Sac1\_C383S interfere with growth in a dominant negative manner. An *L. pneumophila*  $\Delta icmT$  mutant, lacking a functional Icm/Dot T4SS, did not replicate in any of the *D. discoideum* mutant strains (data not shown). Taken together, compared to the parental *D. discoideum* strain, *L. pneumophila* replicates less efficiently in absence of the MCS components Vap or OSBP11 and upon the production of Sac1\_ΔTMD, while the bacteria replicate more efficiently in absence of OSBP8 (**Table 1**).

OSBPL8 was identified on LCVs purified from *L. pneumophila*-infected RAW 264.7 macrophages [55, 56], suggesting that OSBPs and MCS components might also play a role for LCV formation in mammalian cells. To assess the role of MCS components for intracellular replication of *L. pneumophila* in mammalian cells, we used a pharmacological approach and RNA interference. Upon treatment of RAW 264.7 macrophages with the steroidal saponin OSBP inhibitor OSW-1 [65], the intracellular replication of GFP-producing *L. pneumophila* JR32 was significantly inhibited in a dose-dependent manner (**Fig. 3C**). Furthermore, the depletion of Sac1 by RNA interference reduced the intracellular replication of *L. pneumophila* in A549 lung epithelial cells by approximately 25% (**Fig. 3D, Fig. S4BC**), similarly to the depletion of the small GTPase Arf1 used as a positive control [59]. Taken together, pharmacological and RNA interference experiments indicate that MCS components also promote the intracellular replication of *L. pneumophila* in mammalian cells.

## ***D. discoideum* Vap, OSBP11 and Sac1 promote the expansion of PtdIns(4)P-positive LCVs**

Next, we sought to correlate the intracellular replication of *L. pneumophila* in *D. discoideum* lacking MCS components with alterations of the LCVs. To this end, we quantified the LCV area in *D. discoideum* Ax3 and compared it to the LCVs in the  $\Delta vap$ ,  $\Delta osbG$ ,  $\Delta osbH$ ,  $\Delta osbK$  or  $\Delta sey1$  mutants or to LCVs obtained in strain Ax3 upon production of GFP-Sac1\_ΔTMD (**Fig. 4A, Fig. S5A**).

Compared to LCVs in *D. discoideum* Ax3, LCVs in the  $\Delta vap$  strain were significantly smaller at 2 h and 8 h p.i., and larger at 16 h p.i. (**Fig. 4B**). Moreover, the LCVs were significantly smaller in the  $\Delta osbK$  mutant strain at 2 h, 8 h and 16 h p.i., larger in the  $\Delta osbH$  mutant at 8 h and 16 h p.i. and did not change in the  $\Delta osbG$  mutant (**Fig. 4B**). Intriguingly, the LCVs in the  $\Delta osbK$  mutant strain were even smaller than in the  $\Delta sey1$  mutant used as a control [66]. The production of GFP-Sac1\_ΔTMD in *D. discoideum* Ax3 significantly reduced the LCV size at 2 h, 8 h and 16 h post infection compared to amoeba producing GFP-Sac1 or GFP-Sac1\_C383S (**Fig. 4B**). Upon production of GFP-Sac1\_ΔTMD in the  $\Delta vap$ ,  $\Delta osbG$ ,  $\Delta osbH$ ,  $\Delta osbK$ , or  $\Delta sey1$  mutant strains the LCV size was also reduced at all time points p.i. compared to amoebae producing GFP-Sac1 (**Fig. S5B**). Taken together, reduced intracellular replication in some *D. discoideum* strains ( $\Delta vap$ ,  $\Delta osbK$ ,  $\Delta sey1$ , and Sac1\_ΔTMD) is positively correlated with a reduced LCV expansion, and increased intracellular replication in the  $\Delta osbH$  mutant is correlated with an enhanced LCV expansion.

## **Sac1\_ΔTMD reduces the accumulation of PtdIns(4)P, Vap and OSBP8 on LCV-ER MCS**

We then sought to assess the effects of *D. discoideum* MCS components on the LCV PtdIns(4)P levels. To this end, we infected amoeba with either mCerulean- or mPlum-

producing *L. pneumophila* and analyzed PtdIns(4)*P* on LCVs by confocal microscopy and imaging flow cytometry (IFC) using dually labeled *D. discoideum* strains producing P4C-mCherry and either GFP-Sac1 (**Fig. 5AB, Fig. S6**) or GFP-Sac1\_ΔTMD (**Fig. 2A, Fig. 4A, Fig. 5B**, data not shown).

Compared to the ectopic production of GFP-Sac1, the production of GFP-Sac1\_ΔTMD in *D. discoideum* Ax3 resulted in a significant decrease of the IFC P4C colocalization score (see Materials and Methods) for the acquisition of P4C-mCherry on LCV-ER MCS (**Fig. 5B**). GFP-Sac1\_ΔTMD localized in strain Ax3 throughout the cell and does not appear to have an organelle preference (**Fig. 2A, Fig. 4A**). Accordingly, this result suggests that ectopic production of GFP-Sac1\_ΔTMD reduces the PtdIns(4)*P* levels on both the ER as well as the limiting LCV membrane, which cannot be discriminated due to the lower resolution of IFC compared to confocal microscopy. Similarly, the ectopic production of GFP-Sac1\_ΔTMD in the *D. discoideum* Δ*vap*, Δ*osbG*, Δ*osbH*, or Δ*osbK* mutant strains resulted in a decrease of PtdIns(4)*P* on LCV-ER MCS (**Fig. 5B**), while GFP-Sac1\_ΔTMD localized in the mutant strains throughout the cell (data not shown). At the same time the P4C colocalization score on LCV-ER MCS in the Δ*vap*, Δ*osbG*, Δ*osbH*, or Δ*osbK* mutant strains was similar among the mutants but overall higher than on LCVs in the Ax3 parental strain (**Fig. 5B**). These findings suggest that the depletion of a single MCS component suffices to increase the overall levels of PtdIns(4)*P* on LCV-ER MCS.

Upon production of GFP-Sac1 in the *D. discoideum* Δ*vap*, Δ*osbG*, Δ*osbH*, or Δ*osbK* mutant strains, the IFC Sac1 colocalization score was similar for all LCV-ER MCS (**Fig. 5C**). This result indicates that the localization of Sac1 to LCV-ER MCS is not dependent on Vap or the OSBPs tested. The Sac1 colocalization score was slightly (but not significantly) lower in the Δ*sey1* mutant strain, suggesting that Sey1 might play a role in the acquisition of Sac1 to LCV-ER MCS (**Fig. 5C**). This result is reflected in the finding that Sey1 promotes the

recruitment of ER to LCVs [66]. In summary, compared to the production of GFP-Sac1, the production of GFP-Sac1\_ΔTMD in *D. discoideum* Ax3 or the Δvap, ΔosbG, ΔosbH, ΔosbK or Δsey1 mutant strains decreased the PtdIns(4)P level on LCV-ER MCS, while Sac1 did not change, in agreement with the notion that GFP-Sac1\_ΔTMD globally reduces PtdIns(4)P levels.

We also assessed by confocal microscopy and IFC the effect of Sac1\_ΔTMD for the accumulation of Vap, OSBP7, OSBP8 or OSBP11 on LCVs (**Fig. 5DE, Fig. S7**). To this end, we used dually fluorescent labeled *D. discoideum* Ax3 producing either mCherry-Sac1 or mCherry-Sac1\_ΔTMD and GFP fusion proteins of Vap, OSBP7, OSBP8 or OSBP11. Compared to the ectopic production of mCherry-Sac1, the production of mCherry-Sac1\_ΔTMD in *D. discoideum* Ax3 resulted in a significant decrease of the IFC MCS component colocalization score for the acquisition on LCV-ER MCS of GFP fusions of Vap and OSBP8, but not OSBP7, OSBP11 or Sey1 (**Fig. 5E**). Taken together, compared to the production of mCherry-Sac1, the production of mCherry-Sac1\_ΔTMD in *D. discoideum* Ax3, decreased the levels of Vap and OSBP8 on LCV-ER MCS, suggesting that the localization of these MCS components is regulated by PtdIns(4)P levels on the LCVs.

## **The *L. pneumophila* effectors LepB and SidC promote expansion of PtdIns(4)P-positive LCVs**

To assess the role of *L. pneumophila* effector proteins for LCV remodeling and PtdIns(4)P levels, we analyzed LepB, a Rab1 GTPase activating protein (GAP)/PtdIns 4-kinase [20, 31] and SidC, a PtdIns(4)P interactor/ubiquitin ligase [17, 57, 74, 75]. To this end, we quantified the LCV area in *D. discoideum* Ax3 producing CnxA-GFP, GFP-Sac1 or GFP-Sac1\_ΔTMD, following an infection with mCerulean-producing *L. pneumophila* JR32, ΔlepB or ΔsidC (**Fig. 6A, Fig. S8**).

In *D. discoideum* producing CnxA-GFP, LCVs harboring  $\Delta lepB$  or  $\Delta sidC$  mutant *L. pneumophila* were significantly smaller than LCVs harboring strain JR32 at 1 h, 2 h and 8 h p.i. (**Fig. 6B**). Overall, the LCVs were of similar size in *D. discoideum* producing GFP-Sac1, but significantly smaller in *D. discoideum* producing GFP-Sac1 $\Delta$ TMD. In the latter case, LCVs harboring  $\Delta lepB$  or  $\Delta sidC$  mutant *L. pneumophila* were also significantly smaller than LCVs harboring strain JR32 at 1 h, 2 h and 8 h p.i. ( $\Delta lepB$ ) and at 1 h p.i. ( $\Delta sidC$ ).

In order to correlate the LCV area with the PtdIns(4)*P* levels on the pathogen compartment, we used IFC and *D. discoideum* strains producing in parallel P4C-mCherry and CnxA-GFP, GFP-Sac1 or GFP-Sac1 $\Delta$ TMD, infected with mPlum-producing *L. pneumophila* JR32,  $\Delta lepB$  or  $\Delta sidC$  (**Fig. 6C**). In all cases, the IFC colocalization score for the acquisition of P4C-mCherry on LCVs decreased in the course of an infection (1-8 h p.i.). Compared to the parental strain JR32, the score was lowest for  $\Delta lepB$  and intermediate for  $\Delta sidC$ . The colocalization scores were similar in *D. discoideum* producing CnxA-GFP or GFP-Sac1, but significantly lower in *D. discoideum* producing GFP-Sac1 $\Delta$ TMD. Taken together, the lack of the *L. pneumophila* Rab1 GAP/PtdIns 4-kinase LepB or the PtdIns(4)*P* interactor/ubiquitin ligase SidC causes a reduction in LCV area and PtdIns(4)*P* levels. These results indicate that the *L. pneumophila* effector proteins LepB and SidC play a role in the PtdIns(4)*P*-dependent LCV remodeling at LCV-ER MCS.

## Discussion

In this study, we identified several *D. discoideum* MCS components localizing to LCVs (**Fig. 1**). We then used dually fluorescence-labeled *D. discoideum* amoeba to visualize and quantify MCS components at the LCV-ER interface. The protein Vap localized to the PtdIns(4)*P*-positive LCV membrane as well as the ER, while OSBP8 and Sac1 exclusively localized to the ER, and OSBP11 was detected solely on the LCV membrane (**Fig. 2, Table 1**). The MCS

components were found to be implicated in intracellular growth of *L. pneumophila* (**Fig. 3**) and LCV remodeling (**Fig. 4**). Host and bacterial factors regulate the PtdIns(4)*P* levels on LCVs: a derivative of the PtdIns(4)*P* 4-phosphatase Sac1 lacking its membrane anchor, Sac1\_ΔTMD (**Fig. 5**), or the lack of the *L. pneumophila* PtdIns 4-kinase, LepB (**Fig. 6**), reduced the PtdIns(4)*P* score on LCVs. Taken together, these findings are compatible with the notion that a *Legionella*- and host cell-driven PtdIns(4)*P* gradient at LCV-ER MCSs promotes Vap-, Sac1- and OSBP-dependent pathogen vacuole remodeling (**Fig. 7**).

We quantified LCV size changes at early infection time points (1-2 h p.i.) to assess the role of MCS components in LCV remodeling (**Fig. 4, Fig. 6**). This approach revealed that Vap and even more pronouncedly OSBP11 promote LCV expansion. The size reduction of LCVs in *D. discoideum* Δ*vap* or Δ*osbK* mutant strains was relatively small: the LCVs in the mutant strains were ca. 2-2.5 μm<sup>2</sup>, compared to ca. 3 μm<sup>2</sup> in the Ax3 parental strain. Accordingly, these small LCV size changes likely reflect a structural remodeling of the pathogen vacuole rather than a substantial LCV expansion. MCS promote the non-vesicular exchange of lipids in mammalian cells [60], and “counter lipids” transported by OSBPs along a Sac1-dependent PtdIns(4)*P* gradient at ER MCS include phosphatidylserine [63, 64] and cholesterol [61, 65]. The identification of the lipids exchanged by the LCV-ER PtdIns(4)*P* gradient and the specific OSBPs involved will be the subject of future studies.

A massive expansion of the pathogen vacuole at later infection time points (> 8 h p.i.) is required to accommodate intracellular replication of *L. pneumophila* and is likely promoted by vesicle fusion. Indeed, LCV formation implicates the interception of (anterograde and retrograde) vesicular trafficking between the ER and the Golgi apparatus [42-44], and nascent LCVs continuously capture and accumulate PtdIns(4)*P*-positive vesicles from the Golgi apparatus [49]. Further supporting the notion that ER-derived vesicles fuse with LCVs is the finding that the SNARE Sec22b, which promotes fusion of ER-derived vesicles with the *cis*-Golgi, is recruited to LCVs shortly after infection [45, 46]. The fusion requires the *L.*



*pneumophila* effector-mediated activation of Rab1 on LCVs and is mediated by the non-canonical pairing of the v-SNARE Sec22b on the vesicles with PM-derived t-SNAREs such as syntaxin2, -3, -4 and SNAP23 on the LCV [47, 48]. In agreement with this scenario, syntaxins (5, 7A/B, 8A/B, 18), t-SNAREs,  $\alpha$ - and  $\gamma$ -SNAP as well as Vti1A, Vamp7A/B and NsfA were identified on LCVs by proteomics (**Table S1**).

Moreover, several Icm/Dot-translocated *L. pneumophila* effector proteins were identified on LCVs by the comparative proteomics approach (**Table S1**). These effectors prominently include several PtdIns(4)*P*-binding *L. pneumophila* enzymes: the ubiquitin ligase SidC and its paralogue SdcA, the Rab1 GEF/AMPyase SidM/DrrA and the phytate-activated protein kinase Lpg2603. Furthermore, the deAMPyase and SidM antagonist SidD, as well as the retromer interactor RidL were identified on purified LCVs. To study the role of effector proteins for LCV remodeling and PtdIns(4)*P* levels, we analyzed the  $\Delta lepB$  and  $\Delta sidC$  mutant strains (**Fig. 6**). LCVs harboring these mutant strains were smaller and showed a reduced P4C score at LCV-ER MCS. Noteworthy, the effects were augmented in *D. discoideum* producing Sac1\_ΔTMD. These results are readily explicable for the PtdIns 4-kinase LepB: if this kinase is lacking, the PtdIns(4)*P* levels on LCVs are lower and LCV remodeling is impaired. The findings are more difficult to interpret for SidC. This effector localizes exclusively on LCVs in *L. pneumophila*-infected *D. discoideum* [54-57] and tightly binds PtdIns(4)*P* with a dissociation constant,  $K_d$ , in the range of 240 nM [76]. Hence, SidC might titrate PtdIns(4)*P* levels on LCVs, and its absence in *L. pneumophila* is expected to expose more PtdIns(4)*P* on the pathogen vacuole. Accordingly, the finding that LCVs harboring the  $\Delta sidC$  mutant strain show a lower P4C score is caused by more indirect features of the effector.

In addition to the ER-localizing PtdIns(4)*P* 4-phosphatase Sac1, other host cell factors involved in PtdIns(4)*P* turnover might play a role at LCV-ER MCS. The PM-derived PtdIns 4-kinase III $\alpha$  (PI4KIII $\alpha$ ) [22] and trans-Golgi-derived PI4KIII $\beta$  [23] promote the membrane localization of PtdIns(4)*P*-binding effectors, and therefore, might modulate PtdIns(4)*P* levels

on LCVs. Moreover, while the PtdIns(4,5) $P_2$  5-phosphatase OCRL/Dd5P4 produces PtdIns(4) $P$  on LCVs, it restricts intracellular replication of *L. pneumophila* [24, 72], suggesting that this PI phosphatase exerts pleiotropic and complex functions in the context of LCV formation and intracellular bacterial replication.

The association of the LCV with ER in amoeba and macrophages represents a longstanding observation [51, 52], which is not understood on a molecular level. In particular, the identity of the tiny, periodic “hair-like” structures between the pathogen vacuole and the ER is unknown. On a similar note, the identity of possible (bacterial or host) tether proteins is not known. A possible candidate for a *L. pneumophila* tether protein is the Icm/Dot-secreted effector Ceg9. This effector might stabilize the LCV-ER contact sites by directly binding to the host protein Rtn4 [58].

Several intracellular bacterial pathogens hijack MCS components during infection [77]. The mechanistically best characterized case is *Chlamydia trachomatis*, which forms a replication-permissive compartment termed inclusion [77]. Intriguingly, the *Chlamydia* integral membrane proteins IncV and IncD tether the inclusion to the ER [78]. While IncV directly binds Vap on the ER through a FFAT motif [79], IncD indirectly makes contact to Vap through the FFAT motif-containing host protein CERT (ceramide transfer protein) [80, 81].

Taken together, this study has revealed the importance of host and bacterial factors for MCS formation, LCV remodeling and intracellular replication of *L. pneumophila*. The study paves the way for an in-depth functional and structural analysis of LCV-ER MCS, and future studies will identify possible *L. pneumophila* tethering factors, which promote and stabilize the LCV-ER MCS.

## Materials and Methods

### Molecular cloning

All plasmids constructed and used are listed in the Supplementary Information (**Table S2**). Cloning was performed using standard protocols, plasmids were isolated by using commercially available kits from Macherey–Nagel, DNA fragments were amplified using Phusion High Fidelity DNA polymerase. For Gibson assembly, the NEBuilder HiFi DNA assembly kit was used. All constructs were verified by DNA sequencing.

To construct the knockout vectors for *vap*, *osbG*, and *osbK* (**Table S2**), the corresponding 5' fragments were amplified from *D. discoideum* genomic DNA with specific primer pairs oL1277/oL1278, oL1256/oL1356, or oL1687/oL1688, respectively, and cloned into the pBlueScript vector (Stratagene, La Jolla, CA). The 3' fragments were identically produced using the matching primer pairs, oL1279/oL1280, oL1358/oL1359, or oL1693/oL1694, respectively and cloned into pBlueScript containing the 5' fragment. After plasmid sequence verification, the blasticidin resistance cassette was inserted between the two 5' and 3' fragments. The final knockout vectors were digested with KpnI and NotI restriction enzymes before electroporation into Ax3 cells. Blasticidin selection (10 µg/ml) was applied 24 h after transfection. Individual colonies were tested by PCR to confirm gene replacement (**Fig. S3**). The knockout vectors for *osbH* (#629), a kind gift of Prof. Markus Maniak (University of Kassel, Germany), was digested by SpeI and SphI before transfection of Ax3 cells, and transfectants were selected as described above.

The *lepB* deletion strain (IH03) was generated essentially as described [83] by double homologous recombination allelic exchange using counter-selection on sucrose (Suc). The 3' and 5' flanking regions of *lepB* (*lpg2490*) were amplified by PCR using the primer pairs oIH011/oIH013 and oIH012/oIH014, respectively, and genomic *L. pneumophila* DNA as a template. The flanking regions, the Kan<sup>R</sup> cassette and the pLAW344 backbone cut with the appropriate restriction enzymes were assembled using a four-way ligation, yielding the suicide plasmid pIH29. *L. pneumophila* JR32 was transformed by electroporation with pIH29, and co-integration of the plasmid was assayed by selection on CYE/Km (5-7 days, 30°C).

Several clones thus obtained were picked and re-streaked on CYE/Km, grown overnight in AYE medium (96-well plates, 180 rpm) and streaked on CYE/Km/2% Suc. After 3-5 days at 37°C, single colonies were spotted on CYE/Cm, CYE/Km/2% Suc and CYE/Km plates to screen for Cm<sup>S</sup>, Km<sup>R</sup>, Suc<sup>R</sup> colonies. Double-cross-over events (deletion mutants) were confirmed by PCR screening and sequencing.

The constructs pMIB39 (*gfp-osbK*), pMIB41 (*gfp-vap*), pMIB87 (*gfp-osbG*), and pMIB89 (*osbH-gfp*) were constructed by PCR amplification using the primers oMIB38/oMIB39, oMIB14/oMIB12, oMIB20/oMIB18 or oMIB21/oMIB22 and cloned into plasmid pDM317 (*osbK*, *vap*, *osbG*) or pDM323 (*osbH*) after digestion with XhoI/SpeI (*osbK*), BamHI/SpeI (*vap*) or BglII/SpeI (*osbG*, *osbH*).

A GFP-Sac1 fusion was constructed by PCR amplification of the putative open reading frame using *D. discoideum* genomic DNA and the primers oLS039 and oLS040 respectively. The DNA fragment was cloned into BglII and SpeI sites of pDM317, yielding pLS037 (GFP-Sac1). The GFP-Sac1 catalytically inactive mutant (Sac1\_C383S) was obtained exchanging the codon TGT (cysteine) in position 383 to AGC coding for serine. Nucleotide substitution was carried out by site-directed mutagenesis according to the manufacturer's recommendation (QuickChange, Agilent) using pLS037 as template and the PAGE purified primers oSV159 and oSV161 yielding pSV015 (GFP-Sac1\_C383S). The truncated GFP-Sac1\_ΔTMD was obtained by deletion of the transmembrane domain of the *D. discoideum sac1* gene. To this end, pLS037 excluding the transmembrane domain was amplified with the primers oSV227 and oSV228 yielding pSV034. The plasmids pSV044 and pSV045 harboring Sac1 or Sac1\_ΔTMD fused to mCherry were constructed by cloning the genes into BglII and SpeI sites of pDM1042. pLS037 and pSV034 were used as templates.

## Bacteria, cells, growth conditions, and transformation

Bacterial strains and cell lines used are listed in **Table S2**. *L. pneumophila* strains were grown 3 days on charcoal yeast extract (CYE) agar plates, buffered with *N*-(2-acetamido)-2-aminoethane sulfonic acid (ACES) at 37°C. Liquid cultures in ACES yeast extract (AYE) medium were inoculated at an OD<sub>600</sub> of 0.1 and grown at 37°C for 21 h to an early stationary phase (2 x 10<sup>9</sup> bacteria/ml). Chloramphenicol (5 µg/ml) was added as required.

*D. discoideum* stains were grown at 23°C in HL5 medium (ForMedium). Transformation of axenic *D. discoideum* amoeba were performed as described [18, 82]. Blasticidin (10 µg/mL), geneticin (G418, 20 µg/ml) and hygromycin (50 µg/ml) were appropriately added.

Murine macrophage-like RAW 264.7 cells and human A549 lung epithelial carcinoma cells were cultivated in RPMI 1640 medium (Life Technologies) supplemented with 10% heat-inactivated fetal bovine serum (FBS: Life Technologies) and 1% glutamine (Life Technologies). The cells were incubated at 37°C with 5% CO<sub>2</sub> in a humidified atmosphere.

# **Intracellular replication of *Legionella pneumophila***

Intracellular growth of *L. pneumophila* JR32 and  $\Delta icmT$  in different *D. discoideum* strains was assessed by measuring fluorescence increase during intracellular replication of mCherry-producing *Legionella* strains (relative fluorescence units, RFU) and by determining colony-forming units (CFU).

To determine intracellular replication of mCherry-producing *L. pneumophila*, *D. discoideum* amoebae were seeded (2 × 10<sup>4</sup> cells) in 96-well culture-treated plates (Thermo Fisher) and cultured in HL-5 medium at 23°C. The cells were infected (MOI 1) with the *L. pneumophila* strains JR32 or  $\Delta icmT$  harboring plasmid pNP102. After 21 h growth in AYE medium, the bacteria were diluted in MB medium, centrifuged (450 × *g*, 10 min, RT), and incubated for 1 h at 25°C (well plate was kept moist with water in extra wells). Subsequently, infected cells were washed three times with MB medium, incubated for the time indicated at

25°C, and mCherry fluorescence was measured every 2 days using a microtiter plate reader (Synergy H1, Biotek).

To assess CFUs, *D. discoideum* amoebae were infected (MOI 1) with mCherry-producing *L. pneumophila* JR32 or  $\Delta icmT$  grown for 21 h, diluted in MB medium, centrifuged and incubated for 1 h at 25°C. The infected cells were washed three times with MB medium and incubated for the time indicated at 25°C. The infected amoebae were lysed for 10 min with 0.8% saponin (47036, Sigma-Aldrich). Subsequently, serial dilutions were plated every 2 days on CYE agar plated containing Cam (5 µg/ml) and incubated for 3 days at 37°C. CFUs were counted using an automated colony counter (CounterMat Flash 4000, IUL Instruments, CounterMat software) and the number of CFUs (per ml) was calculated.

To test if members of the OSBP family affect intracellular replication of *L. pneumophila* in murine RAW 264.7 macrophages, the steroidal saponin OSBP inhibitor OSW-1 (CAY-30310, Cayman) was added at different concentrations. The macrophages were detached diluted with pre-warmed supplemented RPMI to a concentration of  $2.5 \times 10^4$  cells/140 µL medium and grown for 24 h in 96-well plates. Liquid cultures of GFP-producing *L. pneumophila* JR32 (pNT28) were grown for 21 h and diluted in pre-warmed supplemented RPMI to a concentration of  $5 \times 10^4$  cells/50 µL medium. A 10 µM OSW-1 stock solution was prepared freshly. Bacterial suspensions, the OSW-1 working solution (final concentration 5, 20 or 100 nM) and sterile DPBS were added to wells, yielding an MOI 1. The infection was synchronized by centrifugation ( $450 \times g$ , 10 min.). Plates were incubated at 37°C and 5 % CO<sub>2</sub> in a humidified atmosphere. At the indicated time points (12, 24, 36, 48, 60 h p.i.) intracellular replication was assessed by measuring bacterial GFP production with a plate reader.

## RNA interference, determination of proteins depletion efficiency and cytotoxicity

RNA interference experiments were performed as described [59]. Briefly, A549 cells were treated for 48 h with siRNA oligonucleotides with a final concentration of 10 nM in a 96-well plate (RFU) or 24-well plate (toxicity, Western blot) (**Table S3**). The diluted siRNA was added to the wells (5-10 min) at room temperature (RT), and diluted cells (96-well:  $2 \times 10^4$ , 24-well:  $6 \times 10^4$ ) in RPMI medium with FBS was added on top (48 h). Subsequently, the cells were infected (MOI 10) with GFP-producing *L. pneumophila* strains (pNT28), centrifuged and incubated for 1 h at 37°C with 5% CO<sub>2</sub>, washed three times and incubated for 24 h. GFP fluorescence was measured as described above at 1 h and 24 h post-infection.

Protein depletion efficiency was assessed as follows: cells were harvested in ice-cold PBS and lysed with ice-cold NP-40 cell lysis buffer. Cell extracts were subjected to SDS PAGE. After Western blotting, PVDF membranes were blocked with PBS/5% bovine serum albumin (BSA; Sigma-Aldrich) for 1 h at RT. Subsequently, specific primary antibodies against SacM1L (13033-1-AP, Proteintech) or GAPDH (2118, Cell Signaling) were diluted 1:500 - 1:1,000 in blocking buffer and used to stain the indicated proteins (4°C, overnight). Finally, horse radish peroxidase (HRP)-conjugated secondary antibodies (GE Healthcare Life Sciences) were diluted 1:2,000 in blocking buffer and incubated (1 h, RT). After extensive washing, the enhanced chemiluminescence (ECL) signal was detected with an ImageQuant LAS4000 (GE Healthcare Life Sciences).

To assess cell viability after siRNA treatment, the Zombie Aqua fixable viability kit (BioLegend) was used. A549 cells were grown and treated with siRNA oligonucleotides (**Table S3**) as described above (protein depletion efficiency). Cells treated for 1 h with 70% sterile-filtered ethanol (EtOH) served as positive control for cell death. The cells were then harvested in ice-cold PBS and stained for 30 min in the dark with 50 µl Zombie Aqua dye 1:500 diluted in PBS. Cells were washed once with supplemented RPMI, centrifuged, washed once with PBS, centrifuged and fixed with 4 % paraformaldehyd (PFA) for 30 min at RT. After centrifugation cells were resuspended in 500 µl PBS. Subsequently, cells were subjected



to flow cytometry analysis (BD FACS Canto II). Gates were set according to forward/sideward scatter properties, and 10,000 events were collected for each sample. Mean and standard error of mean (SEM) of Zombie<sup>+</sup> positive cells are shown.

# **Confocal fluorescence microscopy of infected *D. discoideum***

Dually fluorescence labeled *D. discoideum* strains were infected, fixed and imaged by confocal fluorescence microscopy. Prior to infection, exponential phase *D. discoideum* amoebae were seeded ( $1 \times 10^5$  cells per well) in HL5 medium containing geneticin (G418, 20  $\mu$ g/ml) and hygromycin (50  $\mu$ g/ml) in culture treated 6-well plates (VWR) and cultured overnight at 23°C. Cells were infected (MOI 5) with mCerulean-producing *L. pneumophila* JR32 (pNP99), centrifuged ( $450 \times g$ , 10 min, RT) and incubated at 25°C for 1 h. Subsequently, infected cells were washed three times with HL5 medium and incubated at 25°C for the time indicated. At given time points, infected cells (including supernatant) were collected from the 6-wells plate, centrifuged ( $500 \times g$ , 5 min, RT) and fixed with 4% PFA (Electron Microscopy Sciences) for 30 min at RT. Following fixation, the cells were washed twice with PBS, transferred to a 16-wells  $\mu$ -slide dish (Ibidi) and immobilized by adding a layer of PBS/0.5% agarose.

Image acquisition was performed using the confocal microscope Leica TCS SP8 X CLSM (HC PL APO CS2, objective 63 $\times$ /1.4–0.60 oil; Leica Microsystems) with a scanning speed of 200 Hz, bi-directional laser scan. Pictures were acquired with a pixel/voxel size close to the instrument's Nyquist criterion of  $43 \times 43 \times 130$  nm (xyz). Images were deconvolved with Huygens professional version 19.10 software (Scientific Volume Imaging, <http://svi.nl>) using the CMLE algorithm, set to 10-20 iterations and quality threshold of 0.05.

# **Imaging flow cytometry of infected *D. discoideum***

Processing of infected *D. discoideum* for IFC was performed as described [84, 85]. *D. discoideum* cells harboring the plasmids indicated were seeded in a 12-well plate containing HL5 medium, geneticin and hygromycin, and infected (MOI 5) with mPlum-producing *L. pneumophila* JR32,  $\Delta lepB$  or  $\Delta sidC$  (pAW014). The infection was synchronized by centrifugation ( $450 \times g$ , 10 min, RT). The cells were incubated for 1 h at 25°C, washed three times with HL5 and incubated at 25°C. At the indicates time points cells were collected, centrifuged ( $450 \times g$ , 5 min, RT) and fixed in 2 % PFA for 90 min on ice. Fixed infected amoebae were washed twice in phosphate-buffered saline (PBS) and resuspended in 20  $\mu$ l ice cold PBS prior to IFC analysis.

At least 5000 cells were acquired using an imaging flow cytometer (ImageStramX MkII; Amnis) and analyzed with the IDEAS (v6.2) software (Amnis). Infected amoeba containing one intracellular *L. pneumophila* bacterium were gated and assessed for colocalization of GFP and mCherry (host) with mPlum produced by the bacteria. The software computes the IFC colocalization score (bright detail similarity), which is the log-transformed Pearson's correlation coefficient of the localized bright spots with a radius of 3 pixels or less in two images and is used to quantify relative enrichment of a marker on the LCV. Data analysis was performed using GraphPad Prism.

## Comparative proteomics of purified LCVs

LCVs from *D. discoideum* amoebae were purified basically as described [86]. Briefly, *D. discoideum* Ax3 or  $\Delta sey1$  producing CnxA-GFP (pAW016) was seeded in T75 flasks (3 per sample) one day before the experiment to reach 80% confluency. The amoebae were infected (MOI 50, 1 h) with *L. pneumophila* JR32 producing mCherry (pNP102) grown to stationary phase (21 h liquid culture). Subsequently, the cells were washed with SorC buffer and scraped in homogenization buffer (20 mM HEPES, 250 mM sucrose, 0.5 mM EGTA, pH 7.2) [45]. Cells were homogenized using a ball homogenizer (Isobiotec) with an exclusion size of 8  $\mu$ m

and incubated with an anti-SidC antibody followed by a secondary anti-rabbit antibody coupled to magnetic beads. The LCVs were separated in a magnetic field and further purified by a density gradient centrifugation step as described [87]. Three independent biological samples were prepared each for LCVs purified from *L. pneumophila*-infected *D. discoideum* Ax3 or  $\Delta$ sey1.

LCVs purified by immuno-magnetic separation and density gradient centrifugation (fraction 4) were resolved by 1D-SDS-PAGE, the gel lanes were excised in ten equidistant pieces and subjected to trypsin digestion [88]. For the subsequent LC-MS/MS measurements, the digests were separated by reversed phase column chromatography using an EASY nLC 1000 (Thermo Fisher Scientific) with self-packed columns (OD 360  $\mu$ m, ID 100  $\mu$ m, length 20 cm) filled with 3  $\mu$ m diameter C18 particles (Dr. Maisch, Ammerbuch-Entringen, Germany) in a one-column setup. Following loading/ desalting in 0.1% acetic acid in water, the peptides were separated by applying a binary non-linear gradient from 5-53% acetonitrile in 0.1% acetic acid over 82 min. The LC was coupled online to a LTQ Orbitrap Elite mass spectrometer (Thermo Fisher, Bremen, Germany) with a spray voltage of 2.5 kV. After a survey scan in the Orbitrap ( $r = 60,000$ ), MS/MS data were recorded for the twenty most intensive precursor ions in the linear ion trap. Singly charged ions were not considered for MS/MS analysis. The lock mass option was enabled throughout all analyzes.

After mass spectrometric measurement, database search against a database of *Dictyostelium discoideum* and *Legionella pneumophila* Philadelphia downloaded Uniprot on 14/10/2019 (25,478 and 3,024 entries, respectively) as well as label-free quantification (LFQ) was performed using MaxQuant (version 1.6.7.0) (Cox, J and Mann, M (2008). MaxQuant enables high peptide identification rates, individualized p.p.b.-range mass accuracies and proteome-wide protein quantification. Nature Biotechnology 26, 1367–72). Common laboratory contaminants and reversed sequences were included by MaxQuant. Search parameters were set as follows: trypsin/P specific digestion with up to two missed cleavages,

methionine oxidation and N-terminal acetylation as variable modification, match between runs with default parameters enabled. The FDRs (false discovery rates) of protein and PSM (peptide spectrum match) levels were set to 0.01. Two identified unique peptides were required for protein identification. LFQ was performed using the following settings: LFQ minimum ratio count 2 considering only unique for quantification.

Results were filtered for proteins quantified in at least two out of three biological replicates before statistical analysis. Here, two conditions were compared by a student's t-test applying a threshold p-value of 0.01, which was based on all possible permutations. Proteins were considered to be differentially abundant if the log<sub>2</sub>-fold change was greater than |0.8|. "ON/OFF proteins" were defined as being identified in all bioreplicates of one strain whereas the protein was not identified in any replicate of the other strain.

## Statistical methods

Microscopy data analysis was performed using GraphPad Prism. The two-sample Student's t-test (Mann-Whitney test, no assumption of Gaussian distributions) was used. Probability values of less than 0.05, 0.01, and 0.001 were used to show statistically significant differences and are represented with \*, \*\*, or \*\*\*, respectively. The value of "n" represents the number of independent experiments performed or the number of analyzed cells per conditions (**Fig. 4B, Fig. 6B**). For the comparative proteomics, the summarized protein expression values were used for statistical testing of between condition differentially abundant proteins. Empirical Bayes moderated t-tests were applied, as implemented in the R/Bioconductor limma package.

## Data Availability

The MS proteomics data discussed in this publication have been deposited to the ProteomeXchange Consortium via the PRIDE [89] partner repository with the dataset

identifier PXD034490 (Reviewer account details: Username, reviewer\_pxd034490@ebi.ac.uk; Password, JrGWYYBQ).

## Acknowledgements

We would like to thank Markus Maniak for providing the deletion construct for *osbH*, Leoni Swart, Xiaoli Ma, Deise Schäfer, and Iris Hube for help with cloning, and Sebastian Grund for technical support with the preparation of MS samples. Work in the group of H.H. was supported by the Swiss National Science Foundation (SNF; 31003A\_175557, 310030\_207826). Work in the group of D.B. was supported by the Federal Ministry of Education and Research (BMBF; grant 031A410B). Work in the group of C.B. was supported by the DFG and the SFB944 (grant SFB 944/3-P25). Work in the group of F.L. was supported by the Région Occitanie, the Centre National de la Recherche Scientifique (CNRS) and the University of Montpellier (UM). The authors declare no conflict of interest.

## References

1. Newton HJ, Ang DK, van Driel IR, Hartland EL. Molecular pathogenesis of infections caused by *Legionella pneumophila*. Clin Microbiol Rev. 2010;23(2):274-98.
2. Mondino S, Schmidt S, Rolando M, Escoll P, Gomez-Valero L, Buchrieser C. Legionnaires' disease: State of the art knowledge of pathogenesis mechanisms of *Legionella*. Ann Rev Pathol. 2020;15:439-66.
3. Hoffmann C, Harrison CF, Hilbi H. The natural alternative: protozoa as cellular models for *Legionella* infection. Cell Microbiol. 2014;16:15-26.
4. Boamah DK, Zhou G, Ensminger AW, O'Connor TJ. From many hosts, one accidental pathogen: The diverse protozoan hosts of *Legionella*. Front Cell Infect Microbiol. 2017;7:477.

- 692 5. Swart AL, Harrison CF, Eichinger L, Steinert M, Hilbi H. *Acanthamoeba* and  
693 *Dictyostelium* as cellular models for *Legionella* infection. Front Cell Infect Microbiol.  
694 2018;8:61.
- 695 6. Hilbi H, Buchrieser C. Microbe profile: *Legionella pneumophila* - a copycat eukaryote.  
696 Microbiology. 2022;168. doi: 10.1099/mic.0.001142.
- 697 7. Qiu J, Luo ZQ. *Legionella* and *Coxiella* effectors: strength in diversity and activity. Nat  
698 Rev Microbiol. 2017;15:591-605.
- 699 8. Finsel I, Hilbi H. Formation of a pathogen vacuole according to *Legionella pneumophila*:  
700 how to kill one bird with many stones. Cell Microbiol. 2015;17:935-50.
- 701 9. Escoll P, Mondino S, Rolando M, Buchrieser C. Targeting of host organelles by  
702 pathogenic bacteria: a sophisticated subversion strategy. Nat Rev Microbiol. 2016;14:5-  
703 19.
- 704 10. Personnic N, Bärlocher K, Finsel I, Hilbi H. Subversion of retrograde trafficking by  
705 translocated pathogen effectors. Trends Microbiol. 2016;24:450-62.
- 706 11. Bärlocher K, Welin A, Hilbi H. Formation of the *Legionella* replicative compartment at  
707 the crossroads of retrograde trafficking. Front Cell Infect Microbiol. 2017;7:482.
- 708 12. Swart AL, Gomez-Valero L, Buchrieser C, Hilbi H. Evolution and function of bacterial  
709 RCC1 repeat effectors. Cell Microbiol. 2020;22:e13246.
- 710 13. Asrat S, de Jesus DA, Hempstead AD, Ramabhadran V, Isberg RR. Bacterial pathogen  
711 manipulation of host membrane trafficking. Ann Rev Cell Dev Biol. 2014;30:79-109.
- 712 14. Sherwood RK, Roy CR. Autophagy evasion and endoplasmic reticulum subversion: The  
713 Yin and Yang of *Legionella* intracellular infection. Ann Rev Microbiol. 2016;70:413-33.
- 714 15. Steiner B, Weber S, Hilbi H. Formation of the *Legionella*-containing vacuole:  
715 phosphoinositide conversion, GTPase modulation and ER dynamics. Int J Med  
716 Microbiol. 2018;308:49-57.

- 717 16. Swart AL, Hilbi H. Phosphoinositides and the fate of *Legionella* in phagocytes. Front  
718 Immunol. 2020;11:25.
- 719 17. Weber SS, Ragaz C, Reus K, Nyfeler Y, Hilbi H. *Legionella pneumophila* exploits  
720 PI(4)P to anchor secreted effector proteins to the replicative vacuole. PLoS Pathog.  
721 2006;2(5):e46.
- 722 18. Weber S, Wagner M, Hilbi H. Live-cell imaging of phosphoinositide dynamics and  
723 membrane architecture during *Legionella* infection. mBio. 2014;5:e00839-13.
- 724 19. Li G, Liu H, Luo ZQ, Qiu J. Modulation of phagosome phosphoinositide dynamics by a  
725 *Legionella* phosphoinositide 3-kinase. EMBO Rep. 2021;22:e51163.
- 726 20. Dong N, Niu M, Hu L, Yao Q, Zhou R, Shao F. Modulation of membrane  
727 phosphoinositide dynamics by the phosphatidylinositide 4-kinase activity of the  
728 *Legionella* LepB effector. Nat Microbiol. 2016;2:16236.
- 729 21. Hsu F, Zhu W, Brennan L, Tao L, Luo ZQ, Mao Y. Structural basis for substrate  
730 recognition by a unique *Legionella* phosphoinositide phosphatase. Proc Natl Acad Sci U  
731 S A. 2012;109:13567-72.
- 732 22. Hubber A, Arasaki K, Nakatsu F, Hardiman C, Lambright D, De Camilli P, et al. The  
733 machinery at endoplasmic reticulum-plasma membrane contact sites contributes to spatial  
734 regulation of multiple *Legionella* effector proteins. PLoS Pathog. 2014;10:e1004222.
- 735 23. Brombacher E, Urwyler S, Ragaz C, Weber SS, Kami K, Overduin M, et al. Rab1  
736 guanine nucleotide exchange factor SidM is a major phosphatidylinositol 4-phosphate-  
737 binding effector protein of *Legionella pneumophila*. J Biol Chem. 2009;284:4846-56.
- 738 24. Weber SS, Ragaz C, Hilbi H. The inositol polyphosphate 5-phosphatase OCRL1 restricts  
739 intracellular growth of *Legionella*, localizes to the replicative vacuole and binds to the  
740 bacterial effector LpnE. Cell Microbiol. 2009;11:442-60.



25. Schoebel S, Blankenfeldt W, Goody RS, Itzen A. High-affinity binding of phosphatidylinositol 4-phosphate by *Legionella pneumophila* DrrA. EMBO Rep. 2010;11:598-604.
26. Del Campo CM, Mishra AK, Wang YH, Roy CR, Janmey PA, Lambright DG. Structural basis for PI(4)P-specific membrane recruitment of the *Legionella pneumophila* effector DrrA/SidM. Structure. 2014;22:397-408.
27. Hammond GR, Machner MP, Balla T. A novel probe for phosphatidylinositol 4-phosphate reveals multiple pools beyond the Golgi. J Cell Biol. 2014;205:113-26.
28. Machner MP, Isberg RR. Targeting of host Rab GTPase function by the intravacuolar pathogen *Legionella pneumophila*. Dev Cell. 2006;11:47-56.
29. Murata T, Delprato A, Ingmundson A, Toomre DK, Lambright DG, Roy CR. The *Legionella pneumophila* effector protein DrrA is a Rab1 guanine nucleotide-exchange factor. Nat Cell Biol. 2006;8:971-7.
30. Machner MP, Isberg RR. A bifunctional bacterial protein links GDI displacement to Rab1 activation. Science. 2007;318:974-7.
31. Ingmundson A, Delprato A, Lambright DG, Roy CR. *Legionella pneumophila* proteins that regulate Rab1 membrane cycling. Nature. 2007;450:365-9.
32. Suh HY, Lee DW, Lee KH, Ku B, Choi SJ, Woo JS, et al. Structural insights into the dual nucleotide exchange and GDI displacement activity of SidM/DrrA. EMBO J. 2010;29:496-504.
33. Zhu Y, Hu L, Zhou Y, Yao Q, Liu L, Shao F. Structural mechanism of host Rab1 activation by the bifunctional *Legionella* type IV effector SidM/DrrA. Proc Natl Acad Sci U S A. 2010;107:4699-704.
34. Oesterlin LK, Goody RS, Itzen A. Posttranslational modifications of Rab proteins cause effective displacement of GDP dissociation inhibitor. Proc Natl Acad Sci U S A. 2012;109:5621-6.

35. Müller MP, Peters H, Blümer J, Blankenfeldt W, Goody RS, Itzen A. The *Legionella* effector protein DrrA AMPylates the membrane traffic regulator Rab1b. *Science*. 2010;329:946-9.
36. Hardiman CA, Roy CR. AMPylation is critical for Rab1 localization to vacuoles containing *Legionella pneumophila*. *mBio*. 2014;5:e01035-13.
37. Neunuebel MR, Chen Y, Gaspar AH, Backlund PS, Jr., Yergey A, Machner MP. De-AMPylation of the small GTPase Rab1 by the pathogen *Legionella pneumophila*. *Science*. 2011;333:453-6.
38. Tan Y, Luo ZQ. *Legionella pneumophila* SidD is a deAMPyase that modifies Rab1. *Nature*. 2011;475:506-9.
39. Mukherjee S, Liu X, Arasaki K, McDonough J, Galan JE, Roy CR. Modulation of Rab GTPase function by a protein phosphocholine transferase. *Nature*. 2011;477:103-6.
40. Tan Y, Arnold RJ, Luo ZQ. *Legionella pneumophila* regulates the small GTPase Rab1 activity by reversible phosphorylcholine. *Proc Natl Acad Sci U S A*. 2011;108:21212-7.
41. Campanacci V, Mukherjee S, Roy CR, Cherfils J. Structure of the *Legionella* effector AnkX reveals the mechanism of phosphocholine transfer by the FIC domain. *EMBO J*. 2013;32:1469-77.
42. Nagai H, Kagan JC, Zhu X, Kahn RA, Roy CR. A bacterial guanine nucleotide exchange factor activates ARF on *Legionella* phagosomes. *Science*. 2002;295:679-82.
43. Kagan JC, Roy CR. *Legionella* phagosomes intercept vesicular traffic from endoplasmic reticulum exit sites. *Nat Cell Biol*. 2002;4:945-54.
44. Robinson CG, Roy CR. Attachment and fusion of endoplasmic reticulum with vacuoles containing *Legionella pneumophila*. *Cell Microbiol*. 2006;8:793-805.
45. Derre I, Isberg RR. *Legionella pneumophila* replication vacuole formation involves rapid recruitment of proteins of the early secretory system. *Infect Immun*. 2004;72:3048-53.

46. Kagan JC, Stein MP, Pypaert M, Roy CR. *Legionella* subvert the functions of rab1 and sec22b to create a replicative organelle. J Exp Med. 2004;199:1201-11.
47. Arasaki K, Roy CR. *Legionella pneumophila* promotes functional interactions between plasma membrane syntaxins and Sec22b. Traffic. 2010;11:587-600.
48. Arasaki K, Toomre DK, Roy CR. The *Legionella pneumophila* effector DrrA is sufficient to stimulate SNARE-dependent membrane fusion. Cell Host Microbe. 2012;11:46-57.
49. Weber S, Steiner B, Welin A, Hilbi H. *Legionella*-containing vacuoles capture PtdIns(4)P-rich vesicles derived from the Golgi apparatus. mBio. 2018;9:e02420-18.
50. Kawabata M, Matsuo H, Koito T, Murata M, Kubori T, Nagai H, et al. *Legionella* hijacks the host Golgi-to-ER retrograde pathway for the association of Legionella-containing vacuole with the ER. PLoS Pathog. 2021;17:e1009437.
51. Swanson MS, Isberg RR. Association of *Legionella pneumophila* with the macrophage endoplasmic reticulum. Infect Immun. 1995;63:3609-20.
52. Abu Kwaik Y. The phagosome containing *Legionella pneumophila* within the protozoan *Hartmannella vermiformis* is surrounded by the rough endoplasmic reticulum. Appl Environ Microbiol. 1996;62:2022-8.
53. Tilney LG, Harb OS, Connelly PS, Robinson CG, Roy CR. How the parasitic bacterium *Legionella pneumophila* modifies its phagosome and transforms it into rough ER: implications for conversion of plasma membrane to the ER membrane. J Cell Sci. 2001;114:4637-50.
54. Urwyler S, Nyfeler Y, Ragaz C, Lee H, Mueller LN, Aebersold R, et al. Proteome analysis of *Legionella* vacuoles purified by magnetic immunoseparation reveals secretory and endosomal GTPases. Traffic. 2009;10:76-87.
55. Hoffmann C, Finsel I, Otto A, Pfaffinger G, Rothmeier E, Hecker M, et al. Functional analysis of novel Rab GTPases identified in the proteome of purified *Legionella*-containing vacuoles from macrophages. Cell Microbiol. 2014;16:1034-52.

56. Schmölders J, Manske C, Otto A, Hoffmann C, Steiner B, Welin A, et al. Comparative proteomics of purified pathogen vacuoles correlates intracellular replication of *Legionella pneumophila* with the small GTPase Ras-related protein 1 (Rap1). Mol Cell Proteomics. 2017;16:622-41.
57. Ragaz C, Pietsch H, Urwyler S, Tiaden A, Weber SS, Hilbi H. The *Legionella pneumophila* phosphatidylinositol-4 phosphate-binding type IV substrate SidC recruits endoplasmic reticulum vesicles to a replication-permissive vacuole. Cell Microbiol. 2008;10:2416-33.
58. Haenssler E, Ramabhadran V, Murphy CS, Heidtman MI, Isberg RR. Endoplasmic reticulum tubule protein reticulon 4 associates with the *Legionella pneumophila* vacuole and with translocated substrate Ceg9. Infect Immun. 2015;83:3479-89.
59. Steiner B, Swart AL, Welin A, Weber S, Personnic N, Kaech A, et al. ER remodeling by the large GTPase atlastin promotes vacuolar growth of *Legionella pneumophila*. EMBO Rep. 2017;18:1817-36.
60. Pemberton JG, Kim YJ, Balla T. Integrated regulation of the phosphatidylinositol cycle and phosphoinositide-driven lipid transport at ER-PM contact sites. Traffic. 2020;21:200-19.
61. Mesmin B, Bigay J, Moser von Filseck J, Lacas-Gervais S, Drin G, Antonny B. A four-step cycle driven by PI(4)P hydrolysis directs sterol/PI(4)P exchange by the ER-Golgi tether OSBP. Cell. 2013;155:830-43.
62. Zewe JP, Wills RC, Sangappa S, Goulden BD, Hammond GR. SAC1 degrades its lipid substrate PtdIns4P in the endoplasmic reticulum to maintain a steep chemical gradient with donor membranes. eLife. 2018;7.
63. Chung J, Torta F, Masai K, Lucast L, Czapla H, Tanner LB, et al. PI4P/phosphatidylserine countertransport at ORP5- and ORP8-mediated ER-plasma membrane contacts. Science. 2015;349:428-32.

- 845 64. Moser von Filseck J, Copic A, Delfosse V, Vanni S, Jackson CL, Bourguet W, et al.  
846 Phosphatidylserine transport by ORP/Osh proteins is driven by phosphatidylinositol 4-  
847 phosphate. *Science*. 2015;349:432-6.
- 848 65. Mesmin B, Bigay J, Polidori J, Jamecna D, Lacas-Gervais S, Antonny B. Sterol transfer,  
849 PI4P consumption, and control of membrane lipid order by endogenous OSBP. *EMBO J*.  
850 2017;36:3156-74.
- 851 66. Hüsler D, Steiner B, Welin A, Striednig B, Swart AL, Molle V, et al. *Dictyostelium*  
852 lacking the single atlastin homolog Sey1 shows aberrant ER architecture, proteolytic  
853 processes and expansion of the *Legionella*-containing vacuole. *Cell Microbiol*.  
854 2021:e13318.
- 855 67. Rivero F, Kuspa A, Brokamp R, Matzner M, Noegel AA. Interaptin, an actin-binding  
856 protein of the alpha-actinin superfamily in *Dictyostelium discoideum*, is developmentally  
857 and cAMP-regulated and associates with intracellular membrane compartments. *J Cell*  
858 *Biol*. 1998;142:735-50.
- 859 68. Peracino B, Wagner C, Balest A, Balbo A, Pergolizzi B, Noegel AA, et al. Function and  
860 mechanism of action of *Dictyostelium* Nramp1 (Slc11a1) in bacterial infection. *Traffic*.  
861 2006;7:22-38.
- 862 69. Buracco S, Peracino B, Cinquetti R, Signoretto E, Vollero A, Imperiali F, et al.  
863 *Dictyostelium* Nramp1, which is structurally and functionally similar to mammalian  
864 DMT1 transporter, mediates phagosomal iron efflux. *J Cell Sci*. 2015;128:3304-16.
- 865 70. Riyahi TY, Frese F, Steinert M, Omosigho NN, Glockner G, Eichinger L, et al. RpkA, a  
866 highly conserved GPCR with a lipid kinase domain, has a role in phagocytosis and anti-  
867 bacterial defense. *PLoS One*. 2011;6:e27311.
- 868 71. Luo ZQ, Isberg RR. Multiple substrates of the *Legionella pneumophila* Dot/Icm system  
869 identified by interbacterial protein transfer. *Proc Natl Acad Sci U S A*. 2004;101:841-6.

72. Finsel I, Ragaz C, Hoffmann C, Harrison CF, Weber S, van Rahden VA, et al. The *Legionella* effector RidL inhibits retrograde trafficking to promote intracellular replication. *Cell Host Microbe*. 2013;14:38-50.
73. Sreelatha A, Nolan C, Park BC, Pawlowski K, Tomchick DR, Tagliabracci VS. A *Legionella* effector kinase is activated by host inositol hexakisphosphate. *J Biol Chem*. 2020.
74. Hsu F, Luo X, Qiu J, Teng YB, Jin J, Smolka MB, et al. The *Legionella* effector SidC defines a unique family of ubiquitin ligases important for bacterial phagosomal remodeling. *Proc Natl Acad Sci U S A*. 2014;111:10538-43.
75. Luo X, Wasilko DJ, Liu Y, Sun J, Wu X, Luo ZQ, et al. Structure of the *Legionella* virulence factor, SidC reveals a unique PI(4)P-specific binding domain essential for its targeting to the bacterial phagosome. *PLoS Pathog*. 2015;11:e1004965.
76. Dolinsky S, Haneburger I, Cichy A, Hannemann M, Itzen A, Hilbi H. The *Legionella longbeachae* Icm/Dot substrate SidC selectively binds phosphatidylinositol 4-phosphate with nanomolar affinity and promotes pathogen vacuole-endoplasmic reticulum interactions. *Infect Immun*. 2014;82:4021-33.
77. Derre I. Hijacking of membrane contact sites by intracellular bacterial pathogens. *Adv Exp Med Biol*. 2017;997:211-23.
78. Stanhope R, Derre I. Making contact: VAP targeting by intracellular pathogens. *Contact*. 2018;1. doi: 10.1177/2515256418775512.
79. Stanhope R, Flora E, Bayne C, Derre I. IncV, a FFAT motif-containing *Chlamydia* protein, tethers the endoplasmic reticulum to the pathogen-containing vacuole. *Proc Natl Acad Sci U S A*. 2017;114:12039-44.
80. Derre I, Swiss R, Agaisse H. The lipid transfer protein CERT interacts with the *Chlamydia* inclusion protein IncD and participates to ER-*Chlamydia* inclusion membrane contact sites. *PLoS Pathog*. 2011;7:e1002092.

81. Elwell CA, Jiang S, Kim JH, Lee A, Wittmann T, Hanada K, et al. *Chlamydia trachomatis* co-opts GBF1 and CERT to acquire host sphingomyelin for distinct roles during intracellular development. PLoS Pathog. 2011;7:e1002198.
82. Weber S, Hilbi H. Live cell imaging of phosphoinositide dynamics during *Legionella* infection. Methods Mol Biol. 2014;1197:153-67.
83. Tiaden A, Spirig T, Weber SS, Brüggemann H, Bosshard R, Buchrieser C, et al. The *Legionella pneumophila* response regulator LqsR promotes host cell interactions as an element of the virulence regulatory network controlled by RpoS and LetA. Cell Microbiol. 2007;9:2903-20.
84. Welin A, Weber S, Hilbi H. Quantitative imaging flow cytometry of *Legionella*-infected *Dictyostelium* amoebae reveals the impact of retrograde trafficking on pathogen vacuole composition. Appl Environ Microbiol. 2018;84:e00158-18.
85. Welin A, Weber S, Hilbi H. Quantitative imaging flow cytometry of *Legionella*-containing vacuoles in dually fluorescence-labeled *Dictyostelium*. Methods Mol Biol. 2019;1921:161-77.
86. Urwyler S, Finsel I, Ragaz C, Hilbi H. Isolation of *Legionella*-containing vacuoles by immuno-magnetic separation. Curr Prot Cell Biol. 2010;Chapter 3, unit 3 34.
87. Hoffmann C, Finsel I, Hilbi H. Pathogen vacuole purification from *Legionella*-infected amoeba and macrophages. Methods Mol Biol. 2013;954:309-21.
88. Bonn F, Bartel J, Buttner K, Hecker M, Otto A, Becher D. Picking vanished proteins from the void: how to collect and ship/share extremely dilute proteins in a reproducible and highly efficient manner. Anal Chem. 2014;86:7421-7.
89. Perez-Riverol Y, Csordas A, Bai J, Bernal-Llinares M, Hewapathirana S, Kundu DJ, et al. The PRIDE database and related tools and resources in 2019: improving support for quantification data. Nucleic Acids Res. 2019;47:D442-D50.



921 **Table 1.** Features of selected *D. discoideum* MCS components.

MCS component	Colocalization			<i>Legionella</i> Icm <sup>a</sup>
	Calnexin (ER) <sup>a</sup>	P4C (PI4P/LCV) <sup>a</sup>	AmtA (PM/EE) <sup>a</sup>	
Vap	++	++	+	positive
OSBP7 ( <i>osbG</i> )	++/- <sup>b</sup>	-	-	no effect
OSBP8 ( <i>osbH</i> )	++	-	-	negative
OSBP11 ( <i>osbK</i> )	-	++	++	positive
Sac1	++	-	-	no effect
Sac1_C383S	++	-	-	no effect
Sac1_ΔTMD	-	-	-	negative

922 <sup>a</sup> Abbreviations: Icm, intracellular multiplication of *L. pneumophila* in *D. discoideum*  
923 producing the Sac1 variants or lacking *vap*, *osbG*, *osbH* or *osbK*, compared to replication in  
924 the parental strain Ax3; ER, endoplasmic reticulum; EE, early endosome; PI4P/LCV,  
925 phosphatidylinositol 4-phosphate/*Legionella*-containing vacuole; PM, plasma membrane.

926 <sup>b</sup> +: co-localization in *L. pneumophila*-infected cells; -: no co-localization in uninfected cells.

927

## Figure Legends

### Figure 1. *D. discoideum* MCS components localizing to LCVs.

(A) Comparative proteomics was performed by mass spectrometry with LCVs purified from *L. pneumophila*-infected *D. discoideum* Ax3 or  $\Delta$ sey1 (for details see Materials and Methods). Among the total of 3658 eukaryotic or bacterial proteins identified, the Venn diagrams show proteins identified in biological triplicates only on LCVs from *D. discoideum* Ax3 (108 proteins; 74 *D. discoideum*, 34 *L. pneumophila*) or only on LCVs from  $\Delta$ sey1 mutant amoeba (14 proteins; 11 *D. discoideum*, 3 *L. pneumophila*). (B) Imaging flow cytometry (IFC) of *D. discoideum* Ax3 or  $\Delta$ sey1 producing P4C-mCherry (pWS032) and GFP fusion proteins of Vap, OSBP7, OSBP8, OSBP11, or Sac1, infected (MOI 5, 1 h) with mPlum-producing *L. pneumophila* JR32 (pAW014). Mean IFC colocalization score and standard error of mean (SEM) for MCS component GFP fusion proteins for > 5000 LCVs is depicted. The data are representative for three independent experiments (\*\*\*P<0.001).

### Figure 2. *Dictyostelium discoideum* MCS components localize to LCVs and/or ER.

(A) Dually labeled *D. discoideum* amoebae producing MCS components fused to GFP, and either calnexin (CnxA)-mCherry (pAW012), P4C-mCherry (pWS032), or AmtA-mCherry were infected (MOI 5, 2 h) with mCerulean-producing *L. pneumophila* JR32 (pNP99), fixed with 4 % PFA, and imaged by confocal fluorescence microscopy. Merged images are shown. Scale bars: 3  $\mu$ m. The Pearson's correlation coefficient was generated using Coloc 2 from Fiji (ImageJ) and is shown for MCS components fused to GFP with respect to (B) CnxA-mCherry, (C) P4C-mCherry, or (D) AmtA-mCherry.

### Figure 3. MCS components modulate replication of *Legionella pneumophila* in *Dictyostelium discoideum* and mammalian cells.

(A) *D. discoideum* Ax3, or the  $\Delta vap$ ,  $\Delta osbG$ ,  $\Delta osbH$ , or  $\Delta osbK$  mutant strains producing GFP (pDM317) or GFP fusions of the MCS components were infected (MOI 1) with mCherry-producing *L. pneumophila* JR32 (pNP102), and intracellular replication was assessed by relative fluorescence units (RFU). Mean and SEM of three independent experiments are shown (\* $P < 0.05$ ; \*\* $P < 0.01$ ; \*\*\* $P < 0.001$ ). (B) *D. discoideum* Ax3 producing CnxA-GFP (pAW016), GFP-Sac1 (pLS037), GFP-Sac1\_C383S (pSV015) or GFP-Sac1\_ΔTMD (pSV034) were infected (MOI 1) with mCherry-producing *L. pneumophila* JR32 (pNP102), and intracellular replication was assessed by relative fluorescence units (RFU). Mean and SEM of three independent experiments are shown (\*\*\* $P < 0.001$ ). (C) RAW 264.7 macrophages were treated with increasing concentrations of OSW-1 (0-100 nM, 1-60 h), infected (MOI 1) with GFP-producing *L. pneumophila* JR32 (pNT28), and intracellular replication was assessed by relative fluorescence units (RFU). Mean and SEM of three independent experiments are shown (\* $P < 0.05$ ; \*\*\* $P < 0.001$ ). (D) A549 epithelial cells transfected for 48 h with 10 nM siRNA oligonucleotides were infected (MOI 10) with GFP-producing *L. pneumophila* JR32 or  $\Delta icmT$  (pNT28), and intracellular replication was assessed by fluorescence with a microplate reader. Growth after 24 h was compared to growth at 1 h. Mean and SEM of three independent experiments are shown (\*\* $P < 0.01$ ).

**Figure 4. Vap, OSBP11, and Sac1 promote expansion of PtdIns(4)P-positive LCVs.**

(A) Dually labeled *D. discoideum* Ax3,  $\Delta vap$ ,  $\Delta osbG$ ,  $\Delta osbH$ ,  $\Delta osbK$  or  $\Delta sey1$  mutants producing P4C-mCherry (pWS032) and CnxA-GFP (pAW016), or Ax3 producing P4C-mCherry and either GFP-Sac1 (pLS037), GFP-Sac1\_C383S (pSV015) or GFP-Sac1\_ΔTMD (pSV034) were infected (MOI 5, 2-16 h) with mCerulean-producing *L. pneumophila* JR32 (pNP99) and fixed with 4 % PFA. Merged images for the analyzed time points are shown. Scale bars: 3  $\mu$ m. (B) LCV area was measured using ImageJ (n=100-200 per condition from 3

independent biological replicates). Means and SEM of single cells are shown (\*\*P<0.01; \*\*\*P<0.001).

**Figure 5.** Sac1\_ΔTMD reduces the accumulation of PtdIns(4)P, Vap and OSBP8 on LCVs.

(A) Dually labeled *D. discoideum* Ax3, Δvap, ΔosbG, ΔosbH, ΔosbK or Δsey1 mutants producing P4C-mCherry (pWS032) and GFP-Sac1 (pLS037) were infected (MOI 5, 2-16 h) with mCerulean-producing *L. pneumophila* JR32 (pNP99) and fixed with 4 % PFA. Merged images for the analyzed time points are shown. Scale bars: 3 μm. (B, C) Imaging flow cytometry (IFC) analysis of dually labeled *D. discoideum* Ax3, Δvap, ΔosbG, ΔosbH, ΔosbK or Δsey1 mutants producing P4C-mCherry (pWS032) and either GFP-Sac1 (pLS037) or GFP-Sac1\_ΔTMD (pSV034), infected (MOI 5, 2 h) with mPlum-producing *L. pneumophila* JR32 (pAW014). (D) Dually labeled *D. discoideum* Ax3 producing GFP fusions of MCS components and either mCherry-Sac1 (pSV044) or mCherry-Sac1\_ΔTMD (pSV045) were infected (MOI 5, 2 h) with mCerulean-producing *L. pneumophila* JR32 (pNP99) and fixed with 4 % PFA. Merged images for the analyzed time points are shown. Scale bars: 3 μm. (E) IFC analysis of dually labeled *D. discoideum* Ax3 producing GFP fusions of MCS components and either mCherry-Sac1 (pSV044) or mCherry-Sac1\_ΔTMD (pSV045), infected (MOI 5, 2 h) with mPlum-producing *L. pneumophila* JR32 (pAW014). Quantification of (B) P4C-mCherry (C) Sac1-GFP or (E) GFP fusions of MCS components localizing to LCVs at 2 h p.i. Due to the lower resolution of IFC, “LCVs” designates the LCV limiting membrane and tightly attached ER. Number of events per sample, n = 5000. Data represent mean and SEM of three independent experiments (\*P<0.05; \*\*P<0.01; \*\*\*P<0.001).

**Figure 6.** The *L. pneumophila* effectors LepB and SidC determine PtdIns(4)P decoration and expansion of LCVs.

(A) Dually labeled *D. discoideum* Ax3 producing P4C-mCherry (pWS032) and either CnxA-GFP (pAW016), GFP-Sac1 (pLS037), or GFP-Sac1\_ΔTMD (pSV034) were infected (MOI 5, 1-8 h) with mCerulean-producing *L. pneumophila* JR32, Δ*lepB* or Δ*sidC* (pNP99) and fixed with 4 % PFA. Merged images for the analyzed time points are shown. Scale bars: 3 μm. (B) LCV area was measured using ImageJ (n=100-200 per condition). Means and SEM of single cells are shown (\*\*P<0.01; \*\*\*P<0.001). (C) Imaging flow cytometry (IFC) analysis of dually labeled *D. discoideum* Ax3 producing P4C-mCherry (pWS032) and either CnxA-GFP (pAW016), GFP-Sac1 (pLS037), or GFP-Sac1\_ΔTMD (pSV034), infected (MOI 5, 1-8 h) with mPlum-producing *L. pneumophila* JR32 (pAW014). Number of events per sample, n = 5000. Data represent mean and SEM of three independent experiments (\*P<0.05; \*\*P<0.01; \*\*\*P<0.001).

# **Figure 7. Localization and function of host and bacterial factors at LCV-ER MCS.**

In dually fluorescence-labeled *D. discoideum* amoeba MCS components such as Vap, OSBPs and Sac1 localize to the LCV-ER interface. The host proteins Vap, OSBP8, Sac1 and Sey1 localize to the ER, and OSBP11 is detected on the PtdIns(4)P-positive LCV membrane as well as on the PM. The MCS components are implicated in intracellular growth of *L. pneumophila* and LCV remodeling. The PtdIns(4)P 4-phosphatase Sac1 lacking its membrane anchor, Sac1\_ΔTMD, or the lack of the *L. pneumophila* PtdIns(3)P 4-kinase, LepB, reduced the PtdIns(4)P score on LCV-ER MCS. These findings suggest that a *Legionella*- and host cell-driven PtdIns(4)P gradient at LCV-ER MCS promotes Vap-, OSBP- and Sac1-dependent pathogen vacuole remodeling.

## **Supplementary Figures**

**Figure S1.** Phylogenetic tree of short OSBPs from *D. discoideum*, *Saccharomyces cerevisiae* and humans.

Sequences of all proteins were either derived from dictybase.org or uniprot and aligned with MAFFT (<https://mafft.cbrc.jp>) using the G-INS-I strategy, unalignlevel 0.8 and “leave gappy regions” to generate a phylogenetic tree in phylo.ilo using NJ conserved sites and the JTT substitution model. Numbers on the branches indicate bootstrap support for nodes from 100 bootstrap replicates.

**Figure S2.** *Dictyostelium discoideum* MCS components localize to LCVs and/or ER.

(A) Dually labeled *D. discoideum* amoebae producing MCS components fused to GFP and either CnxA-mCherry (pAW016), P4C-mCherry (pWS032), or AmtA-mCherry were infected (MOI 5, 2 h) with mCerulean-producing *L. pneumophila* JR32 (pNP99), fixed with 4 % PFA, and imaged by confocal fluorescence microscopy. Single channels are shown. scale bars: 3  $\mu$ m. The Pearson’s correlation coefficient of uninfected cells was generated using Coloc 2 from Fiji (ImageJ) and is shown for MCS components fused to GFP with respect to (B) CnxA-mCherry, (C) P4C-mCherry, or (D) AmtA-mCherry. Data represent mean and SEM of three independent experiments (\*P<0.05; \*\*\*P<0.001).

**Figure S3.** Construction of *D. discoideum* deletion mutants.

Schematic representation of the strategies followed for the construction of *D. discoideum* strains lacking (A) *osbG*, (B) *osbH*, (C) *osbK*, or (D) *vap*, and PCR-based validation.

**Figure S4.** MCS components modulate replication of *L. pneumophila* in *D. discoideum* and mammalian cells.

(A) *D. discoideum* Ax3, or  $\Delta vap$ ,  $\Delta osbG$ ,  $\Delta osbH$ , or  $\Delta osbK$  mutants producing GFP-Sac1 (pLS037) or GFP-Sac1 $\Delta$ TMD (pSV034) were infected (MOI 1) with mCherry-producing *L. pneumophila* JR32 (pNP102), and intracellular replication was assessed by colony-forming units (CFU). Mean and SEM of three independent experiments are shown (\*P<0.05;

**\*\*P<0.01; \*\*\*P<0.001).** To improve clarity, the different mutant strains are shown in separate graphs, each depicting the same data for Ax3/GFP-Sac1. **(B)** Cytotoxicity toward A549 cells of oligonucleotides targeting Arf1 and Sac1 (10 nM siRNA, 48 h) was determined by the Zombie Aqua fixable viability kit (BioLegend) using flow cytometry. Percentage of Zombie-positive cells is shown (means and SEM of triplicate experiments). Untreated cells were used as a negative control, and treatment with 70% EtOH for 1 h served as positive control for cell death. **(C)** A549 epithelial cells were treated with oligonucleotides targeting Sac1 (10 nM siRNA, 48 h), and the efficiency of protein depletion was assessed by Western blot (WB) with the antibodies indicated. Qiagen AllStars unspecific oligonucleotides (“Scrambled”, “Scr”) were used to control for off-target effects, and GAPDH served as WB loading control. Data are representative of two independent experiments.

**Figure S5.** Vap, OSBP11, and Sac1 promote expansion of PtdIns(4)P-positive LCVs.

**(A)** Dually labeled *D. discoideum* Ax3,  $\Delta vap$ ,  $\Delta osbG$ ,  $\Delta osbH$ ,  $\Delta osbK$  or  $\Delta sey1$  mutants producing P4C-mCherry (pWS032) and CnxA-GFP (pAW016), or Ax3 producing P4C-mCherry and either GFP-Sac1 (pLS037), GFP-Sac1\_C383S (pSV015) or GFP-Sac1\_ΔTMD (pSV034) were infected (MOI 5, 2-16 h) with mCerulean-producing *L. pneumophila* JR32 (pNP99) and fixed with 4 % PFA. Single channels for the analyzed time points are shown. Scale bars: 3 μm. **(B)** LCV area was measured using ImageJ (n=100-200 per condition from 3 independent biological replicates). Means and SEM of single cells are shown (\*P<0.05; \*\*P<0.01; \*\*\*P<0.001). The data for Ax3/GFP-Sac1 and Ax3/GFP Sac1\_ΔTMD is also shown in Fig. 4B.

**Figure S6.** Localization of GFP-Sac1 in *D. discoideum* Ax3 or strains lacking MCS components.

Dually labeled *D. discoideum* Ax3,  $\Delta vap$ ,  $\Delta osbG$ ,  $\Delta osbH$ ,  $\Delta osbK$  or  $\Delta seyI$  mutants producing P4C-mCherry (pWS032) and GFP-Sac1 (pLS037) were infected (MOI 5, 2-16 h) with mCerulean-producing *L. pneumophila* JR32 (pNP99) and fixed with 4 % PFA. Single channels for the analyzed time points are shown. Scale bars: 3  $\mu$ m.

**Figure S7.** Localization of GFP-MCS components in *D. discoideum* wild-type producing Sac1 or Sac1\_ $\Delta$ TMD.

Dually labeled *D. discoideum* Ax3 producing GFP fusions of MCS proteins and either mCherry-Sac1 (pSV044) or mCherry-Sac1\_ $\Delta$ TMD (pSV045) were infected (MOI 5, 2 h) with mCerulean-producing *L. pneumophila* JR32 (pNP99) and fixed with 4 % PFA. Single channels for the analyzed time points are shown. Scale bars: 3  $\mu$ m.

**Figure S8.** The *L. pneumophila* effectors LepB and SidC determine PtdIns(4)*P* decoration and expansion of LCVs.

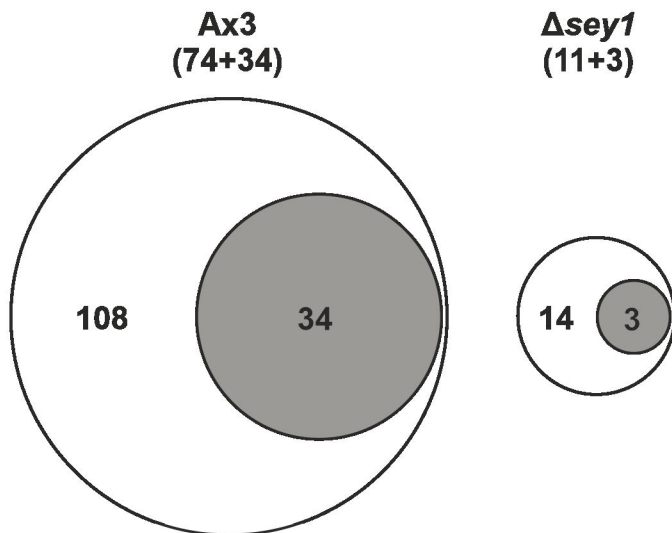
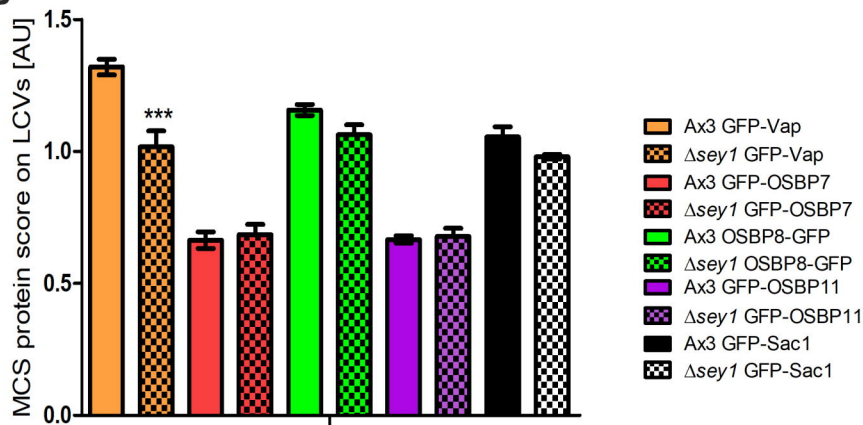
Dually labeled *D. discoideum* Ax3 producing P4C-mCherry (pWS032) and either CnxA-GFP (pAW016), GFP-Sac1 (pLS037), or GFP-Sac1\_ $\Delta$ TMD (pSV034) were infected (MOI 5, 1-8 h) with mCerulean-producing *L. pneumophila* JR32,  $\Delta lepB$  or  $\Delta sidC$  (pNP99) and fixed with 4 % PFA. Single channels for the analyzed time points are shown. Scale bars: 3  $\mu$ m.

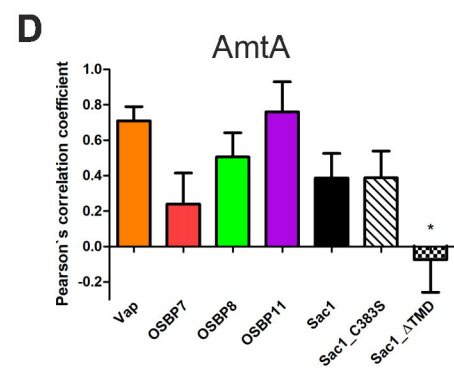
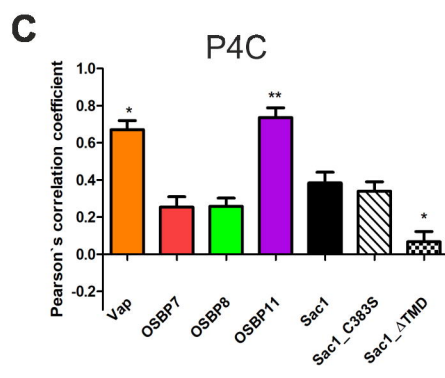
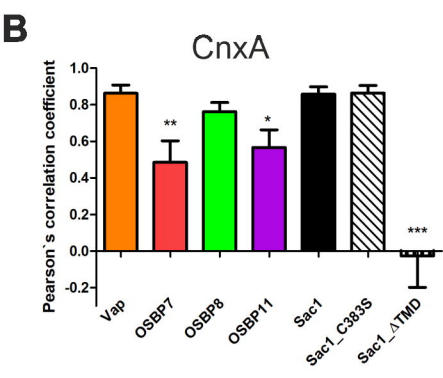
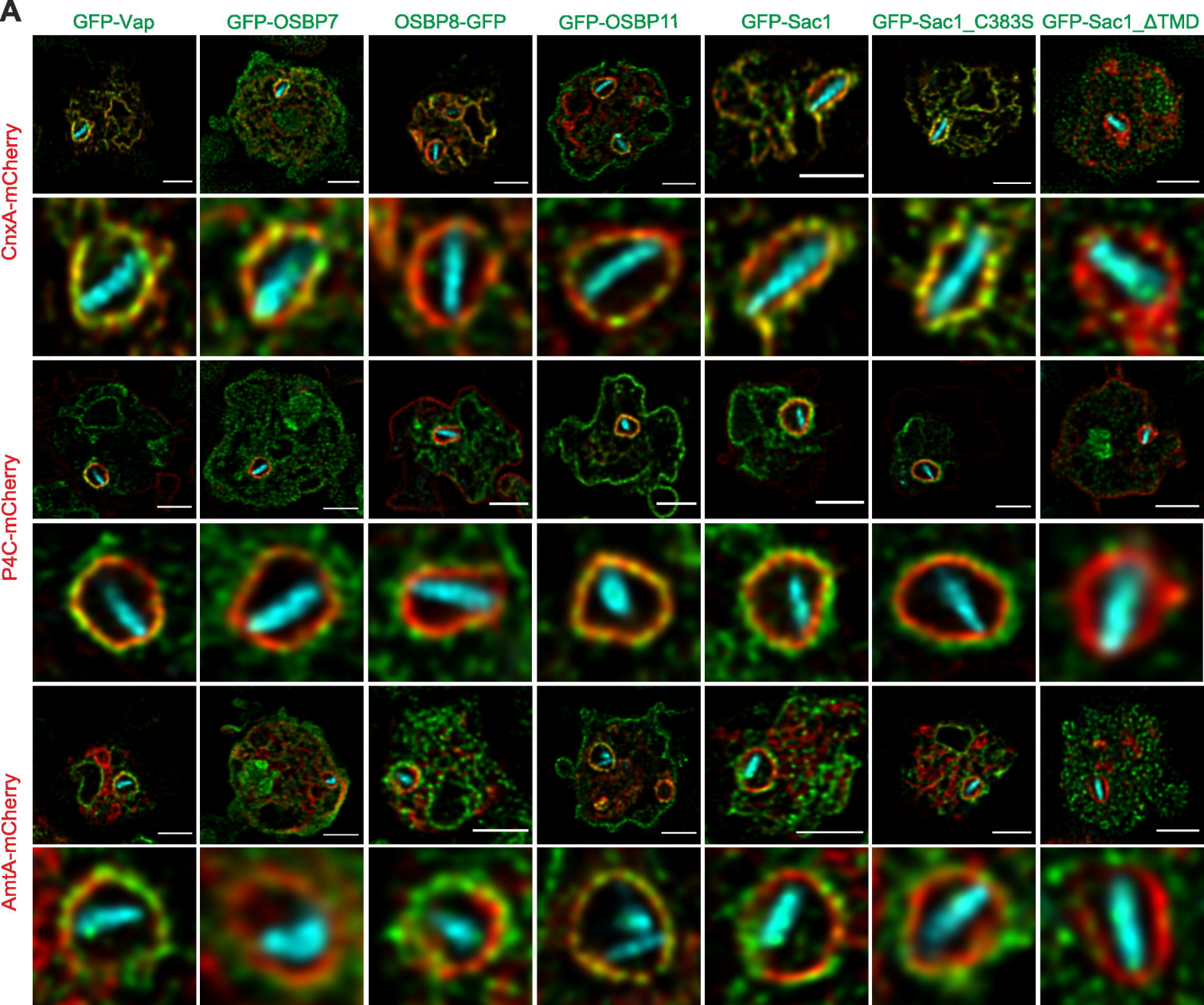
**Table S1.** Comparative proteomics of LCVs from *D. discoideum* Ax3 and  $\Delta seyI$ .

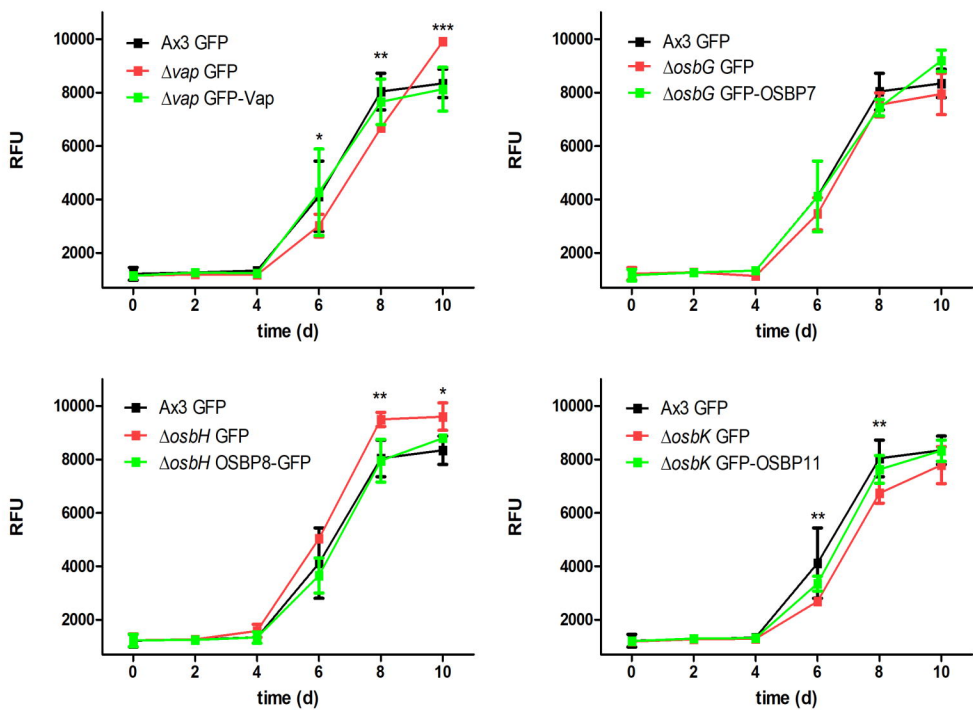
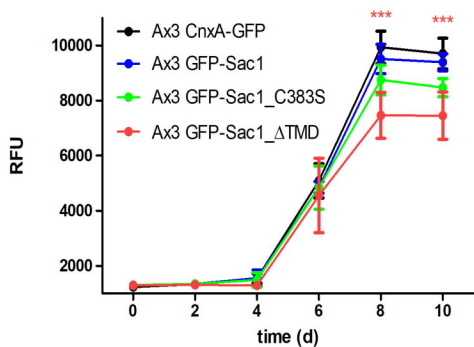
**Table S2.** Cells, bacterial strains, and plasmids used in this study.

**Table S3.** Oligonucleotides used in this study.

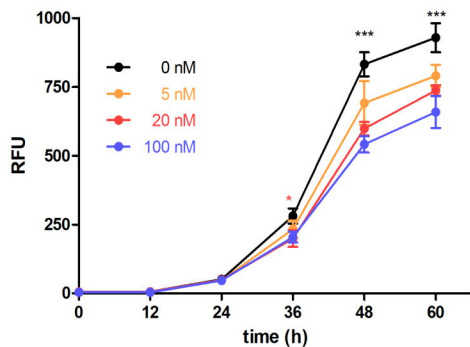


**A****B**

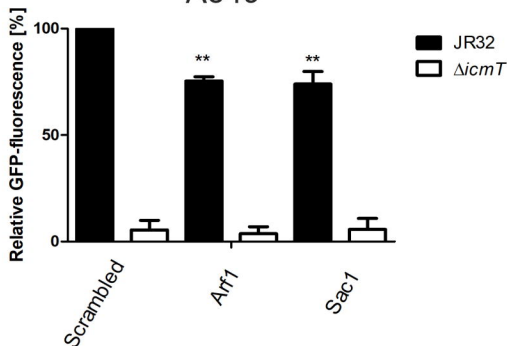


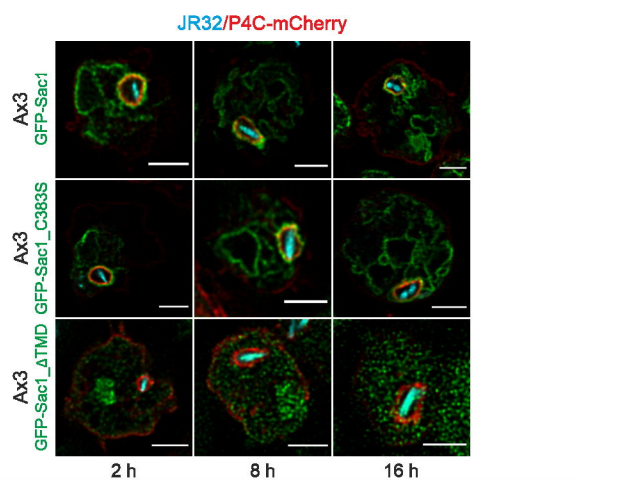
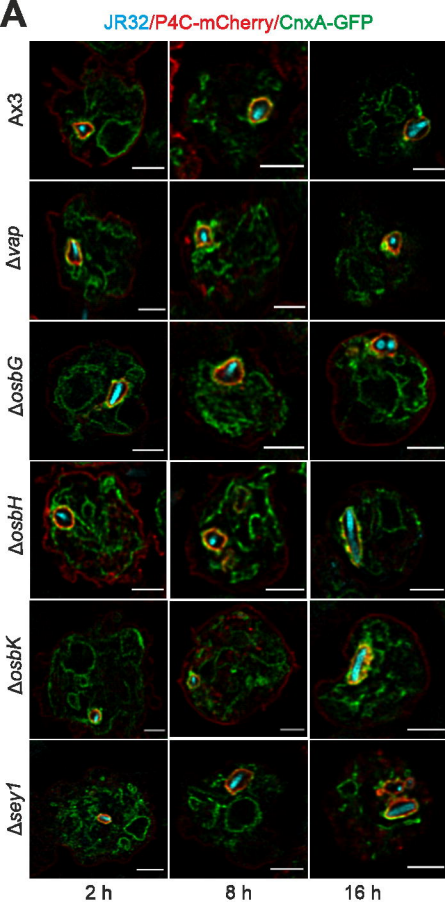
**A***D. discoideum***B***D. discoideum***C**

## RAW 264.7

**D**

## A549





**B**

